Model Blind Primordial Scalar Power Spectrum Reconstruction In Light Of CMB Lensing

Rajorshi Sushovan Chandra
Institute : IUCAA, Pune
Supervisor : Professor Tarun Souradeep

November 17, 2022

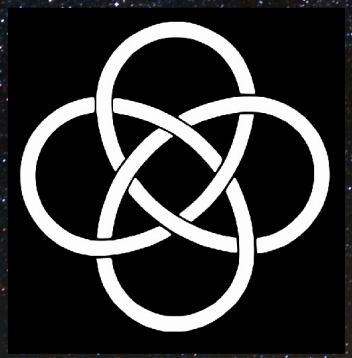

Overview

CMB Introduction : Observables

CMB Weak Lensing Introduction : Observables

Richardson-Lucy Deconvolution Algorithm For $P_R(k)$ Reconstruction

$P_R(k)$ Reconstruction From Lensed Temperature Power Spectrum with Iterative Delensing

Results

Conclusions

CMB Temperature Anisotropy Map

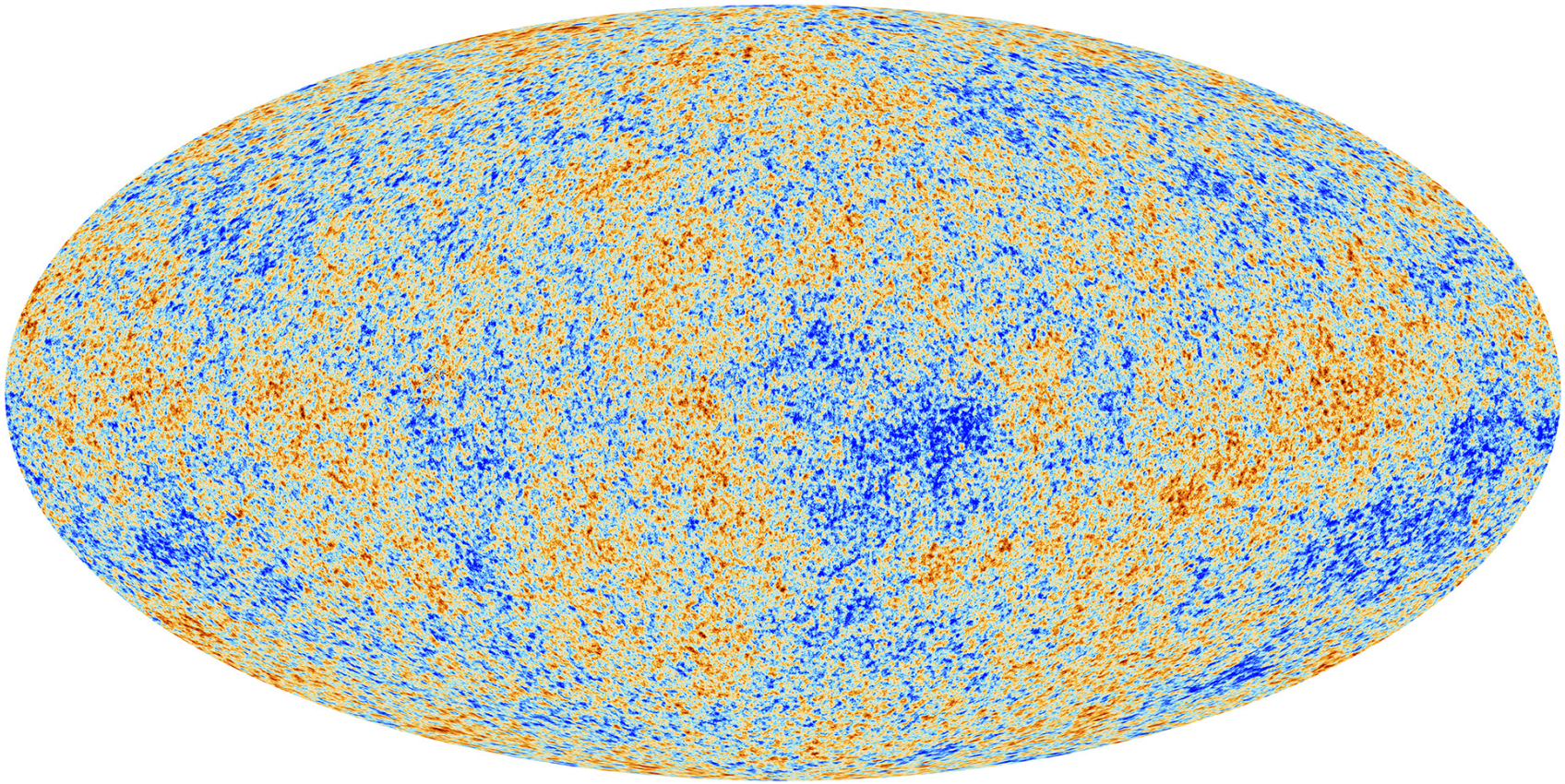

Figure 1: CMB Temperature Anisotropy Full Sky Map

[**Aghanim:2015xee**] Aghanim, N. and others

Observed CMB TT Power Spectrum

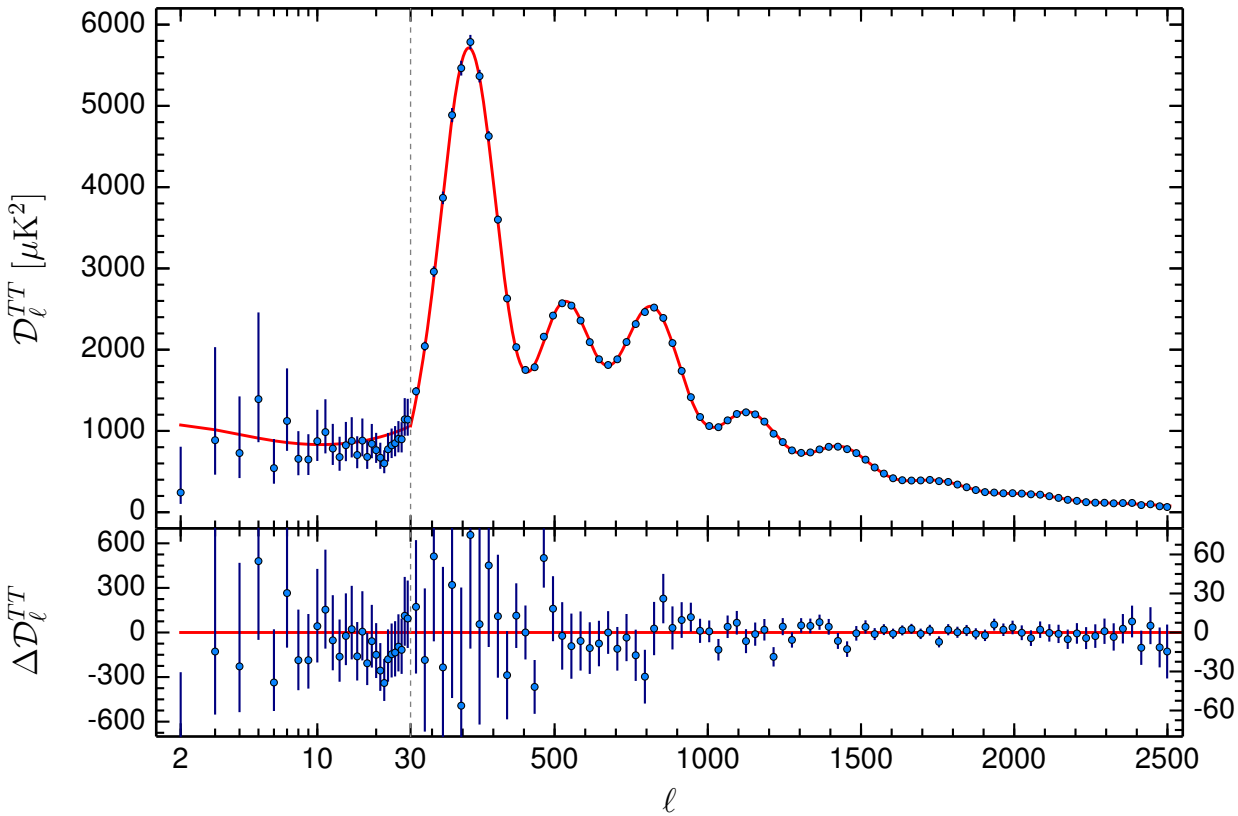

Figure 2: TT Power Spectrum

[**Aghanim:2015xee**] Aghanim, N. and others

$$C_L^{TT} = \int d(\ln k)\mathcal{P}_{\mathcal{R}}(k)|T_L^{(S)}(k)|^2, C_L^{TT} = \sum_k P_k G_{Lk}^{TT} \quad (1)$$

CMB Temperature Anisotropy Evolution Kernel

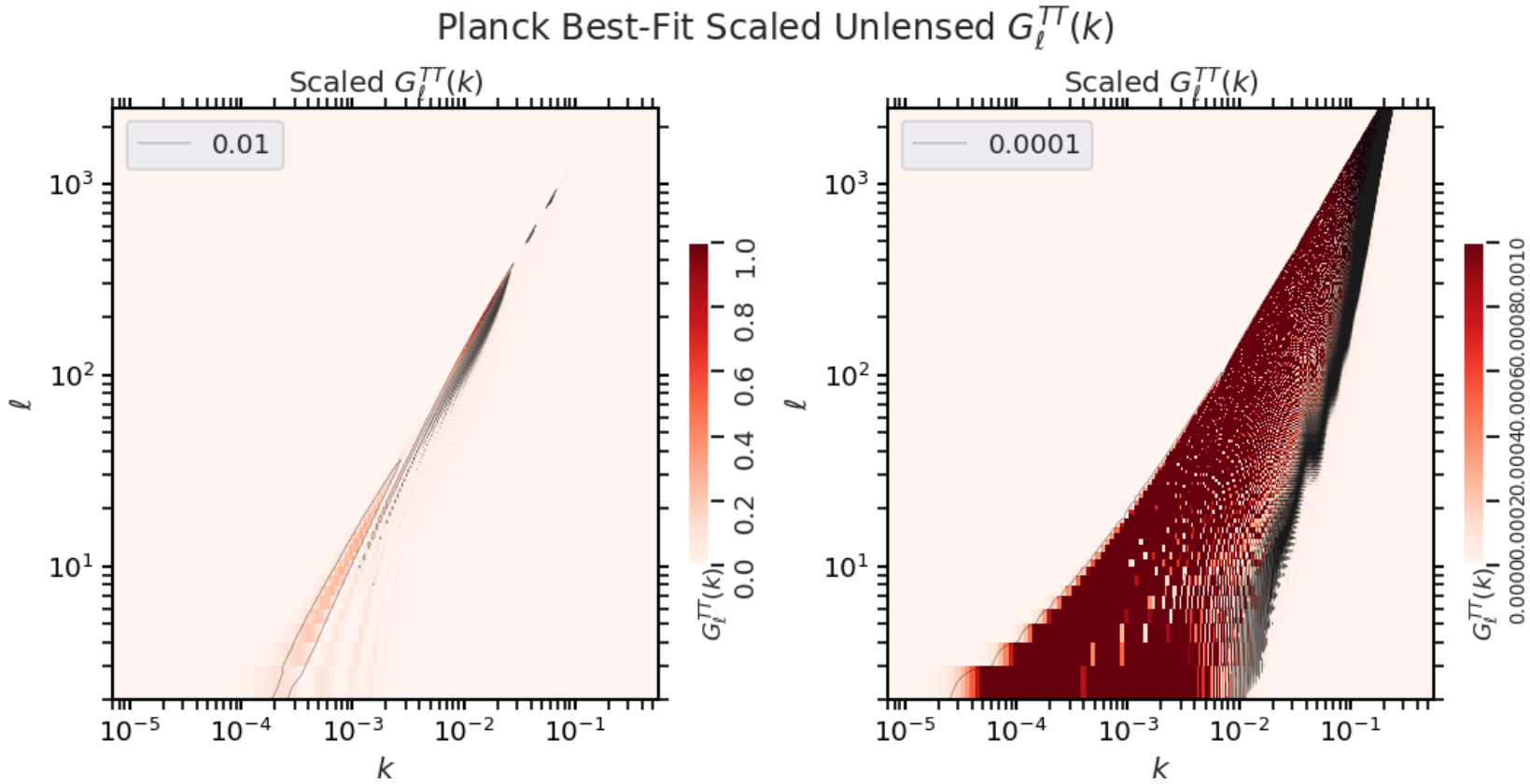

Figure 3: This plot shows a top-down view of the scaled transfer function given by $G_\ell^{TT}(k)/G_\ell^{TT}(k)_{max}$, scaled to a maximum power value of 1. The first plot shows the function with the complete power range 0 to 1 on the colorbar and a power level contour of 0.01. The second plot shows the function in a power range 0 upto 0.001 on the colorbar with a power level contour of 0.0001.

CMB Temperature Anisotropy Evolution Kernel

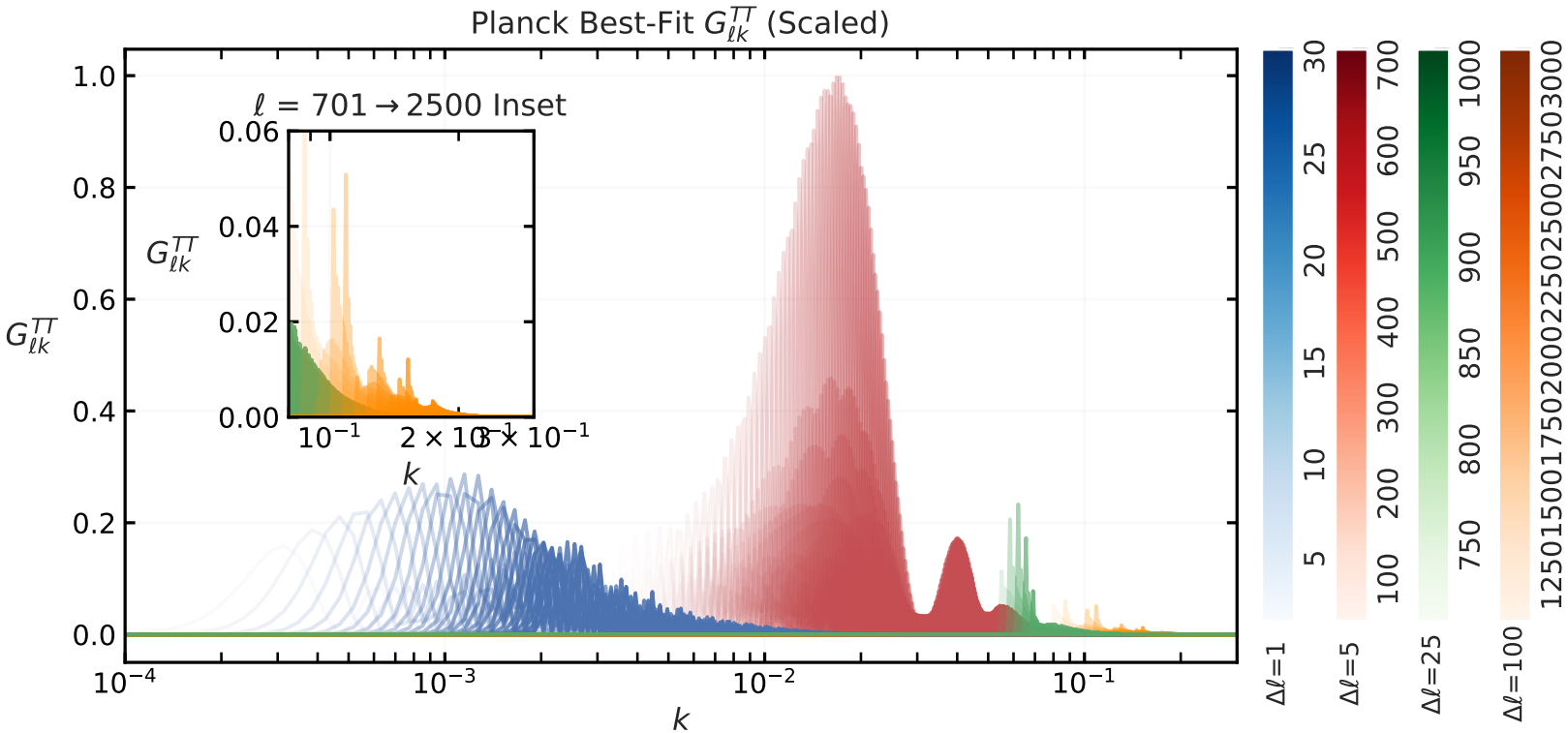

Figure 4: The plot shows the kernel with the numerical integration step size multiplied $G_{\ell k}^{TT} = G_{\ell}^{TT}(k)\Delta k$, projected onto the k vs $G_{\ell}^{TT}(k)$ plane where ℓ is parametrized as a color gradient within blocks of ℓ with corresponding $\Delta\ell$ step sizes showing the plotted frequency of ℓ blocks. The ℓ blocks are roughly segmented by the relative amount of power they transfer.

Weak Lensing Of CMB Over Cosmological Evolution

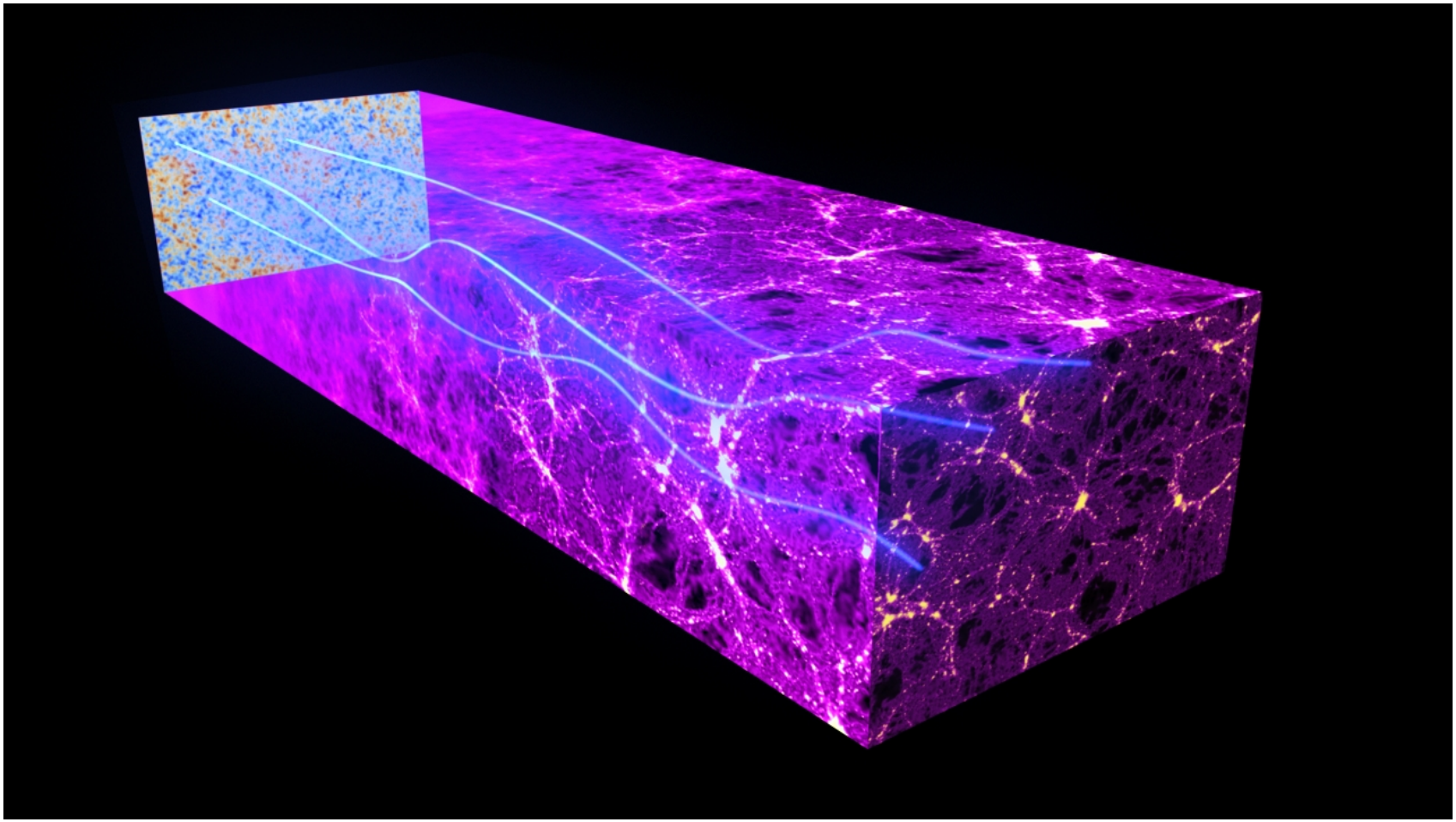

Figure 5: Weak Gravitational Lensing of CMB Photons

Unlensed CMB Map Representation

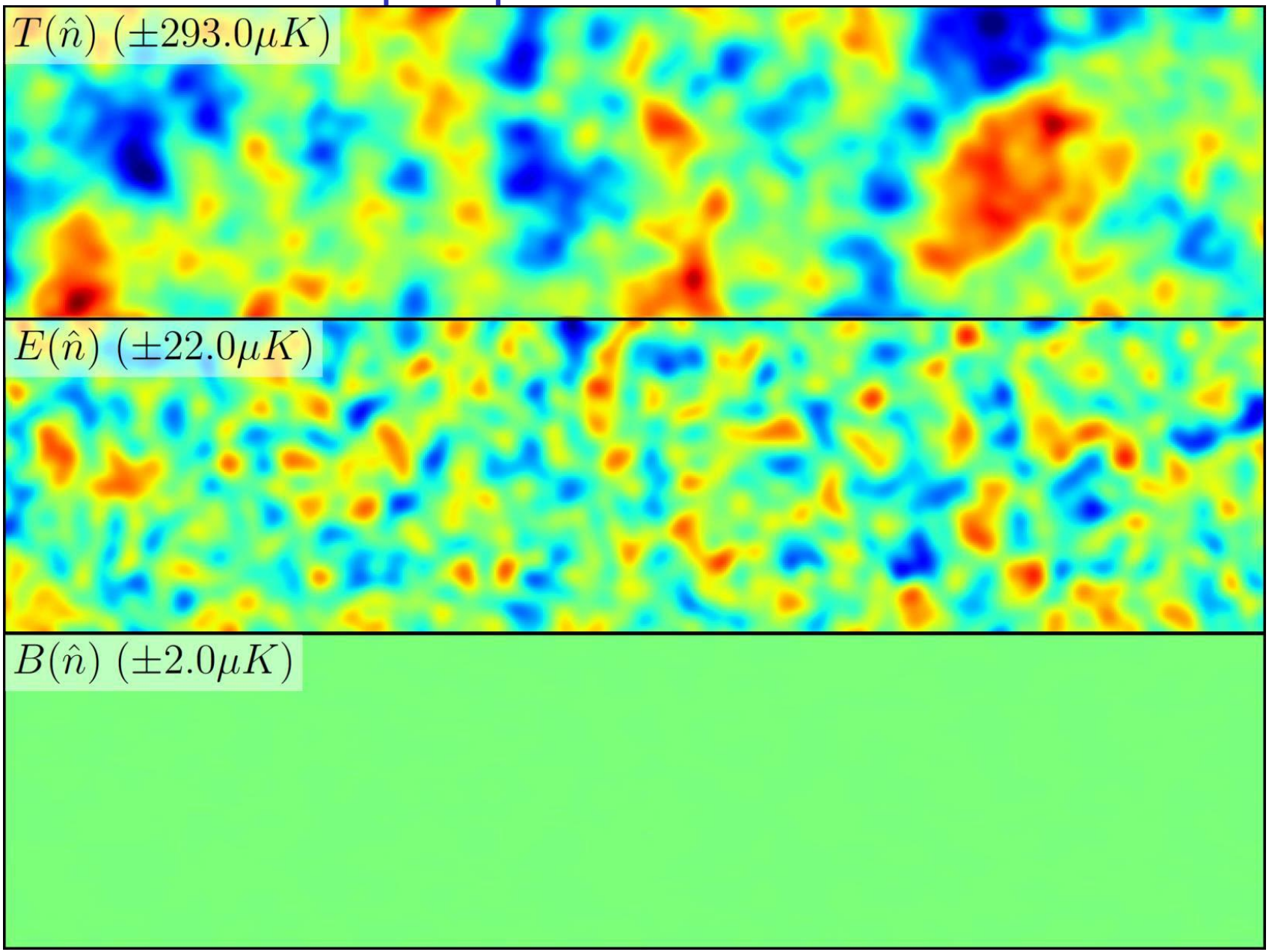

Figure 6: Unlensed CMB Fields, Credits : D. Hanson

Lensed CMB Map Representation

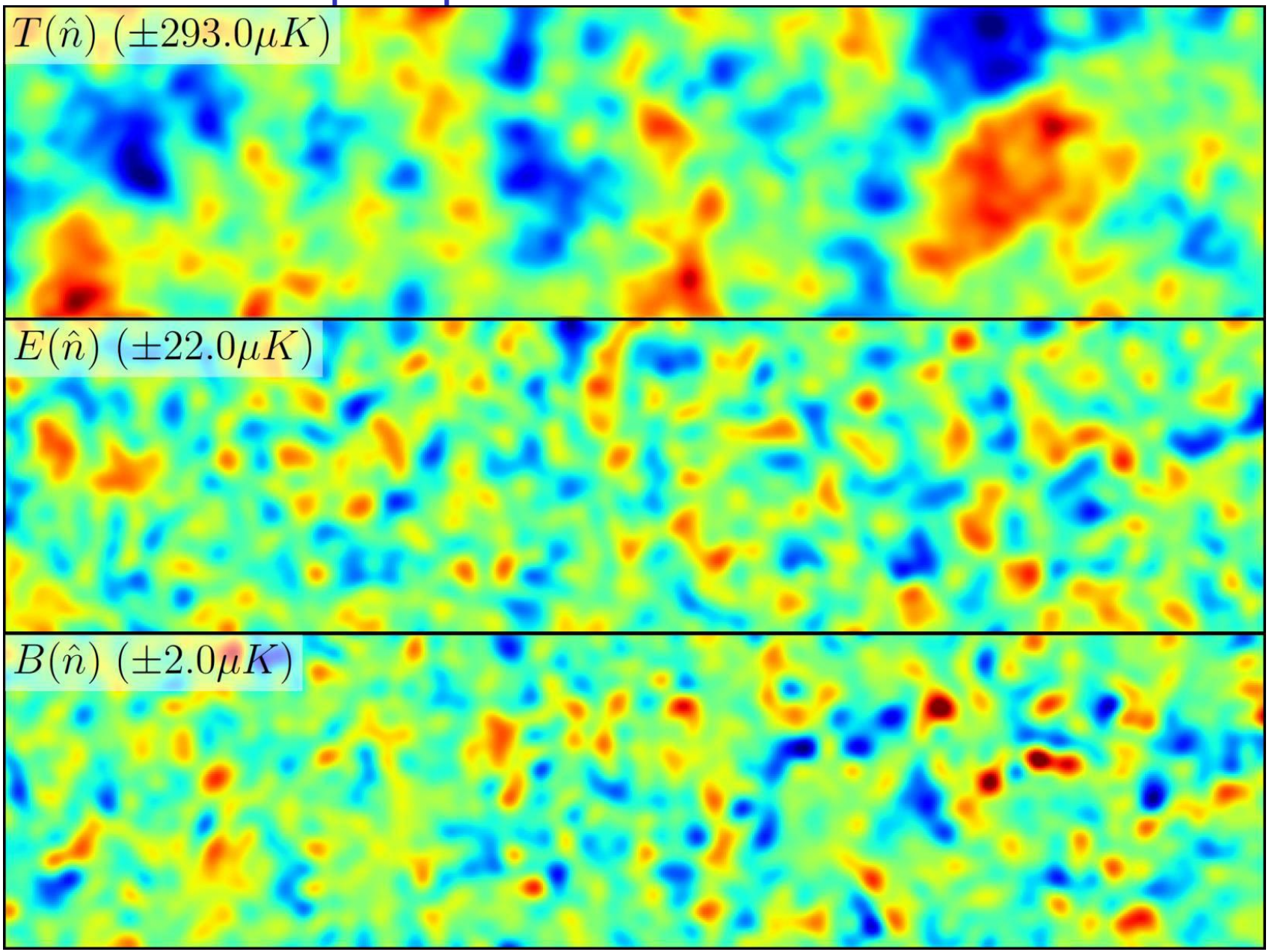

Figure 7: Lensed CMB Fields, Credits : D. Hanson

Why CMB Weak Lensing ?

- Lensing is a carrier of information about fundamental physics
- Lensing is also a contaminant of other observables that carry information about said fundamental physics
- Lensing power spectra $C_L^{\phi\phi}$, map $\phi(\hat{\mathbf{n}})$ carry information about cosmological parameters such as w, Σm_ν
- Lensing needs to be cleaned from other spectra, for example to search for primordial B-modes from C_L^{BB}, parametrized by the tensor-to-scalar ratio r.

Gravitational Lensing in Cosmology

Projected Weak Lensing Map, Power Spectrum

$$\Phi(\mathbf{k};\eta) = T_\Phi(k;\eta)\mathcal{R}(k).$$

$$\phi(\hat{n}) = -2\int_0^{\chi_*} \Phi(\chi\hat{n};\eta_0-\chi)\frac{(\chi_*-\chi)}{(\chi_*\chi)}d\chi$$

$$C_L^{\phi\phi} = 4\pi\int P_R(k)\left[\int_0^{\chi_*} 2T_\phi(k;\eta_0-\chi)\left(\frac{(\chi_*-\chi)}{\chi_*\chi}\right)j_L(k\chi)d\chi\right]^2\frac{dk}{k}$$

Observed Temperature Anisotropy Map, Power Spectrum, (Lensed)

$$\widetilde{\Theta}(\hat{\mathbf{n}}) = \Theta(\hat{\mathbf{n}}') = \Theta(\hat{\mathbf{n}}+\vec{\nabla}\phi(\hat{\mathbf{n}})).$$

$$\widetilde{C}_l^{TT} = C_l^{TT} + C_l^{TT}\sum_{l_1} C_{l_1}^{\phi\phi} S_{ll_1}^{(b)} + \sum_{l_1 l_2} C_{l_1}^{\phi\phi} C_{l_2}^{TT} S_{ll_1l_2}^{(a)}$$

Inflation, Primordial Scalar Perturbations

$$\mathcal{R}_{\mathbf{k}} = \Psi_{\mathbf{k}} + H\frac{\delta\varphi_{\mathbf{k}}}{\dot{\varphi}}$$

$$\mathcal{P}_\mathcal{R}(k) = A_s\left(\frac{k}{k_*}\right)^{n_s-1}$$

Primary Temperature Anisotropy Map, Power Spectrum, (Unlensed)

$$\Theta(\hat{\mathbf{n}}) = \frac{\Delta T(\hat{\mathbf{n}})}{T_o}$$

$$C_L^{TT} = \int d(\ln k)\mathcal{P}_\mathcal{R}(k)|T_L^{(S)}(k)|^2$$

Background Image Credit: Nicolle R. Fuller, National Science Foundation

Gravitational Lensing in Cosmology

Inflation,
Primordial Scalar Perturbations

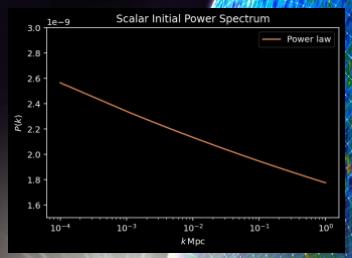

Projected Weak Lensing Map,
Power Spectrum

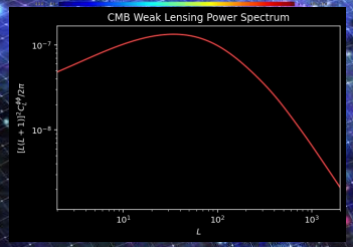

Primary Temperature Anisotropy Map,
Power Spectrum,
(Unlensed)

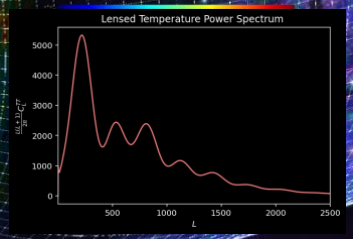

Observed Temperature Anisotropy Map,
Power Spectrum,
(Lensed)

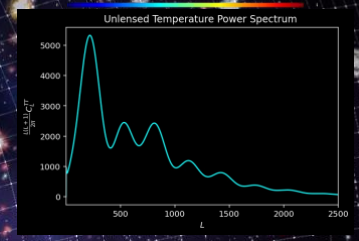

Lensing vs Unlensed, Relative Difference

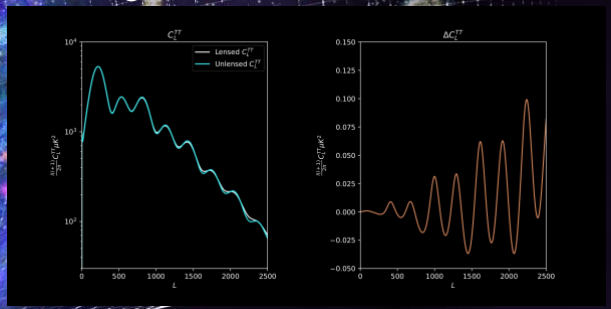

All cosmological power spectra generated using CAMB (Lewis, Challinor, Lasenby, DOI: 10.1086/309179)
All maps generated using Healpix (The healpix primer, Gorski, Wandelt, Hansen, Hivon, Banday, astro-ph/9905275)

Gravitational Lensing in Cosmology

Projected Weak Lensing Map,
Power Spectrum

Observed Temperature Anisotropy Map,
Power Spectrum,
(Lensed)

Inflation,
Primordial Scalar Perturbations

Primary Temperature Anisotropy Map,
Power Spectrum,
(Unlensed)

?

?

All maps and figures obtained from N. Aghanim et al.
"Planck 2018 results. I. Overview and the cosmological legacy of Planck". In: Astron. Astrophys. 641 (2020), A1.
"Planck 2018 results. V. CMB power spectra and likelihoods". In: Astron. Astrophys. 641 (2020), A5.
"Planck 2018 results. VIII. Gravitational lensing". In: Astron. Astrophys. 641 (2020), A8.
"Planck 2018 results. X. Constraints on inflation". In: Astron. Astrophys. 641 (2020), A10.

Why Study Free-Form $P_R(k)$ Reconstruction ?

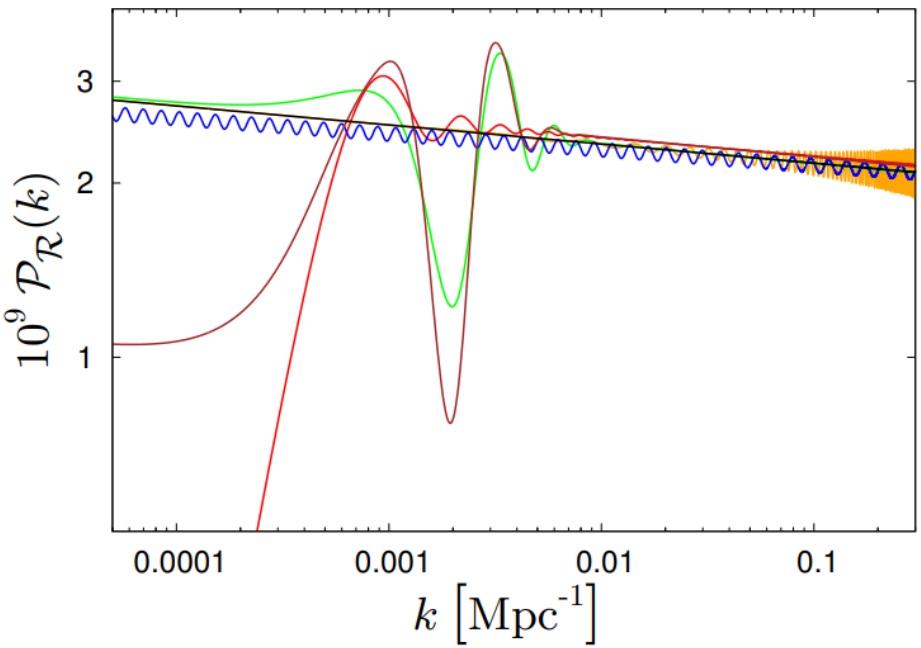

Fig. 33. Best-fit power spectra for the power-law (black curve), step (green), logarithmic oscillation (blue), linear oscillation (orange), and cutoff (red) models using *Planck* TT+lowP data. The brown curve is the best fit for a model with a step in the warp *and* potential (Eqs. 71–80).

Planck 2015 results. XX. Constraints on inflation, Planck Collaboration • P.A.R. Ade (Cardiff U.) et al., DOI: 10.1051/0004-6361/201525898

Brief History of Free-Form Richardson-Lucy $P_R(k)$ Reconstruction

- Originally proposed for CMB power spectrum deconvolution in Arman Shafieloo and Tarun Souradeep. "Primordial power spectrum from WMAP". In: Phys. Rev. D 70 (2004), p. 043523.
- Free-form estimation of $P_R(k)$ for model independent deconvolution
- Further developed on Planck data most recently by Dhiraj Kumar Hazra, Arman Shafieloo, and Tarun Souradeep. "Primordial power spectrum from Planck". In: JCAP 11 (2014), p. 011.

WMAP And Planck Reconstructions

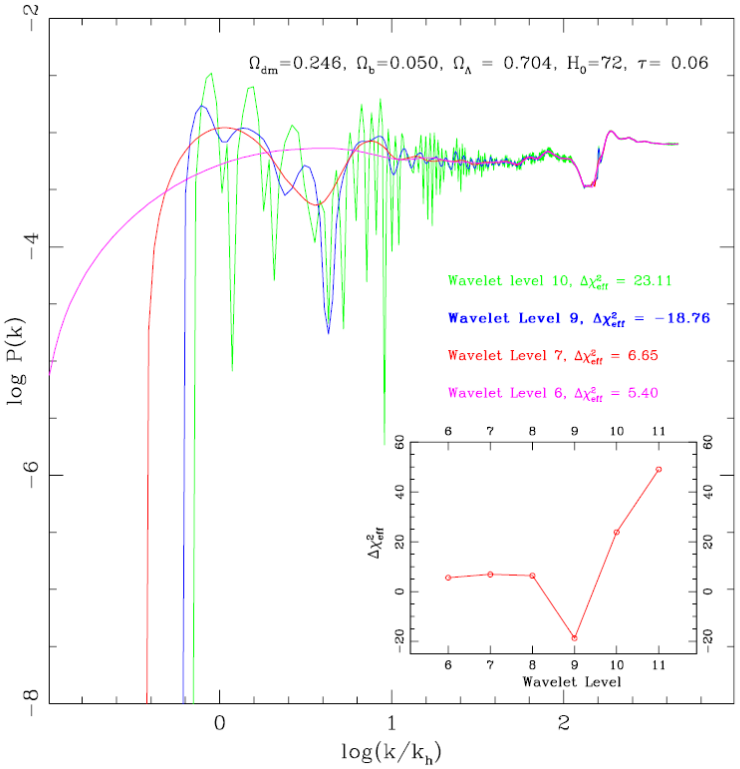

Arman Shafieloo and Tarun Souradeep. “Estimation of Primordial Spectrum with post-WMAP 3 year data”. In: Phys. Rev. D 78 (2008), p. 023511.

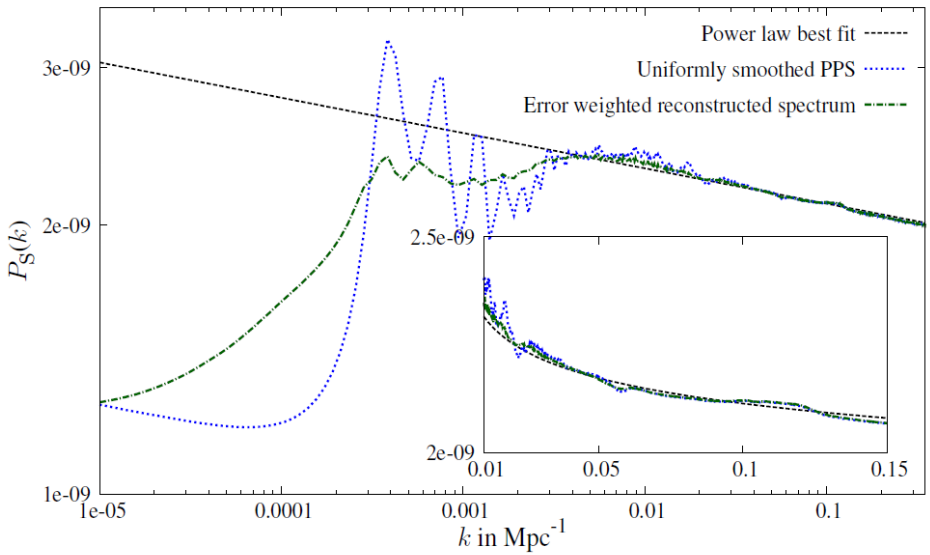

Dhiraj Kumar Hazra, Arman Shafieloo, and Tarun Souradeep. “Primordial power spectrum from Planck”. In: JCAP 11 (2014), p. 011.

Richardson-Lucy Reconstruction Algorithm

$$
\begin{aligned}
P_k^{(i+1)} =& P_k^{(i)} \Bigg[1 + \sum_L \tilde{G}_{Lk}^{\kappa\kappa} \left(\frac{\hat{C}_L^{\kappa\kappa}}{C_L^{\kappa\kappa(i)}} - 1 \right) \tanh^2 \big([\hat{C}_L^{\kappa\kappa} - C_L^{\kappa\kappa(i)}] \\
& \Sigma^{-1} [\hat{C}_L^{\kappa\kappa} - C_L^{\kappa\kappa(i)}]^T \big) \Bigg] \\
=& P_k^{(i)} \left[1 + \sum_L \tilde{G}_{Lk}^{\kappa\kappa} \left(\frac{\hat{C}_L^{\kappa\kappa}}{C_L^{\kappa\kappa(i)}} - 1 \right) \tanh^2 \left(\frac{\hat{C}_L^{\kappa\kappa} - C_L^{\kappa\kappa(i)}}{\hat{\sigma}_L} \right)^2 \right]
\end{aligned}
$$

$\tilde{G}_{Lk}^{\kappa\kappa}$: Discretized Kernel normalised over L

$\hat{C}_L^{\kappa\kappa}$: Data $C_L^{\kappa\kappa}$

Σ^{-1} : Error covariance matric of the data $\hat{C}_L^{\kappa\kappa}$

$$
C_L^{\kappa\kappa(i)} = \sum_k G_{Lk}^{\kappa\kappa} P_k^{(i)} \tag{10}
$$

Following Arman Shafieloo and Tarun Souradeep. “Estimation of Primordial Spectrum with post-WMAP 3 year data”. In: Phys. Rev. D 78 (2008), p. 023511.

Temperature Anisotropy Lensing Power Spectra Comparison

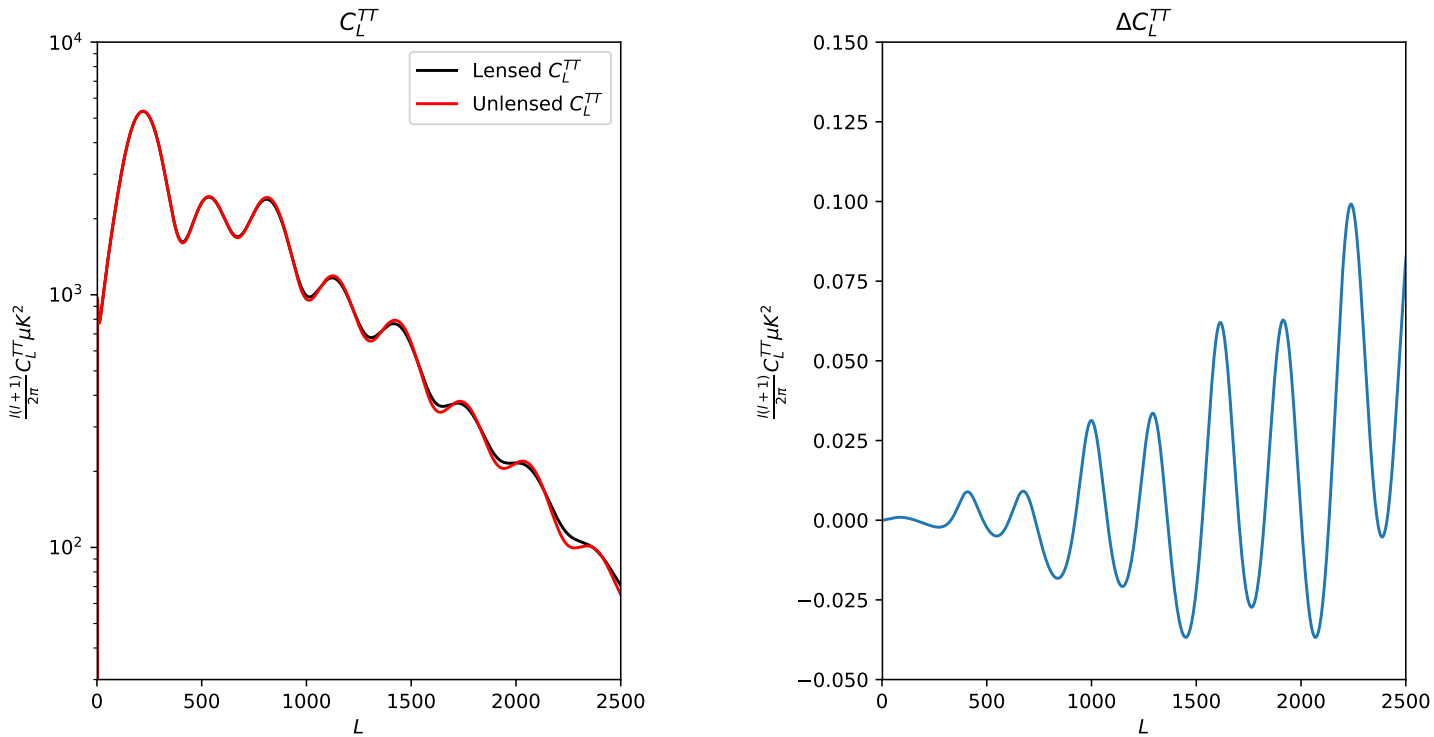

Figure 31: Lensed and unlensed power spectrum and the fractional change in power due to lensing at different scales. (Simulated Using CAMB)

Iterative Delensing For $P_R(k)$ Recovery From C_L^{TT}

$$\tilde{C}_L^{TT} = C_L^{TT} + C_L^{TT} \sum_{l_1} C_{l_1}^{\phi\phi} S_{Ll_1}^{(b)} + \sum_{l_1 l_2} C_{l_1}^{\phi\phi} C_{l_2}^{TT} S_{Ll_1 l_2}^{(a)} \tag{12}$$

$$C_L^{TT} = \sum_k P_k G_{Lk}^{TT}, \; C_L^{\phi\phi} = \sum_{k_1} P_{k_1} G_{Lk_1}^{\phi\phi}, \; \tilde{C}_L^{TT} = \sum_k P_k \tilde{G}_{Lk}^{TT} \tag{13}$$

Where

$$\begin{aligned} \tilde{G}_{Lk}^{TT} =& G_{Lk}^{TT} \left[1 + \sum_{k_1} P_{k_1} \sum_{l_1} G_{l_1 k_1}^{\phi\phi} S_{Ll_1}^{(b)} \right] \\ &+ \left[\sum_{k_1} P_{k_1} \sum_{l_1 l_2} G_{l_1 k_1}^{\phi\phi} G_{l_2 k}^{TT} S_{Ll_1 l_2}^{(a)} \right] \end{aligned} \tag{14}$$

Non-Linear Iterative Richardson-Lucy(NIRL) Algorithm

$$
\begin{aligned}
P_k^{(i+1)} &= P_k^{(i)}\left[1+\sum_l \hat{\tilde{G}}_{lk}^{TT(i)}\left(\frac{\hat{C}_l^{TT}}{C_l^{TT(i)}}-1\right)\right] \\
\hat{\tilde{G}}_{lk}^{TT(i)} &= G_{lk}^{TT}+\Delta G_{lk}^{TT}(P_k^{(i)}) \\
\hat{C}_l^{TT} &: \text{Lensed } C_l^{TT} \text{ Data} \\
C_l^{TT(i)} &= \sum_k \hat{\tilde{G}}_{lk}^{TT(i)} P_k^{(i)},
\end{aligned}
\tag{18}
$$

Where

$$
\begin{aligned}
\tilde{G}_{Lk}^{TT(i)} =& G_{Lk}^{TT}\left[1+\sum_{k_1} P_{k_1}^{(i)} \sum_{l_1} G_{l_1 k_1}^{\phi\phi} S_{L l_1}^{(b)}\right] \\
&+\left[\sum_{k_1} P_{k_1}^{(i)} \sum_{l_1 l_2} G_{l_1 k_1}^{\phi\phi} G_{l_2 k}^{TT} S_{L l_1 l_2}^{(a)}\right]
\end{aligned}
\tag{19}
$$

(Chandra and Souradeep, arXiv:2112.14008)

Default RL $P_R(k)$ Reconstruction on Lensed $\tilde{C}_L^{TT}$

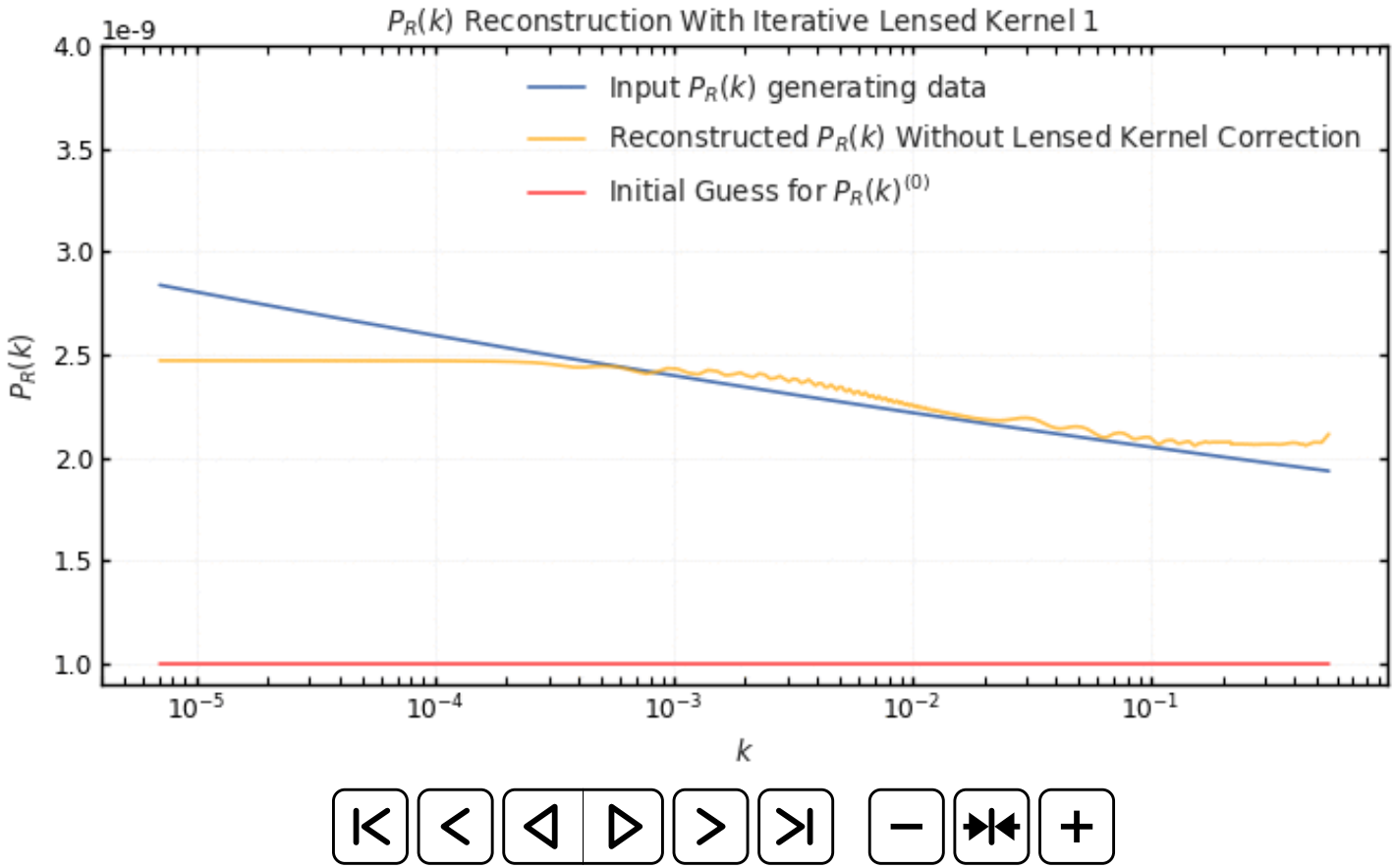

NIRL $P_R(k)$ Reconstruction on Lensed $\tilde{C}_L^{TT}$

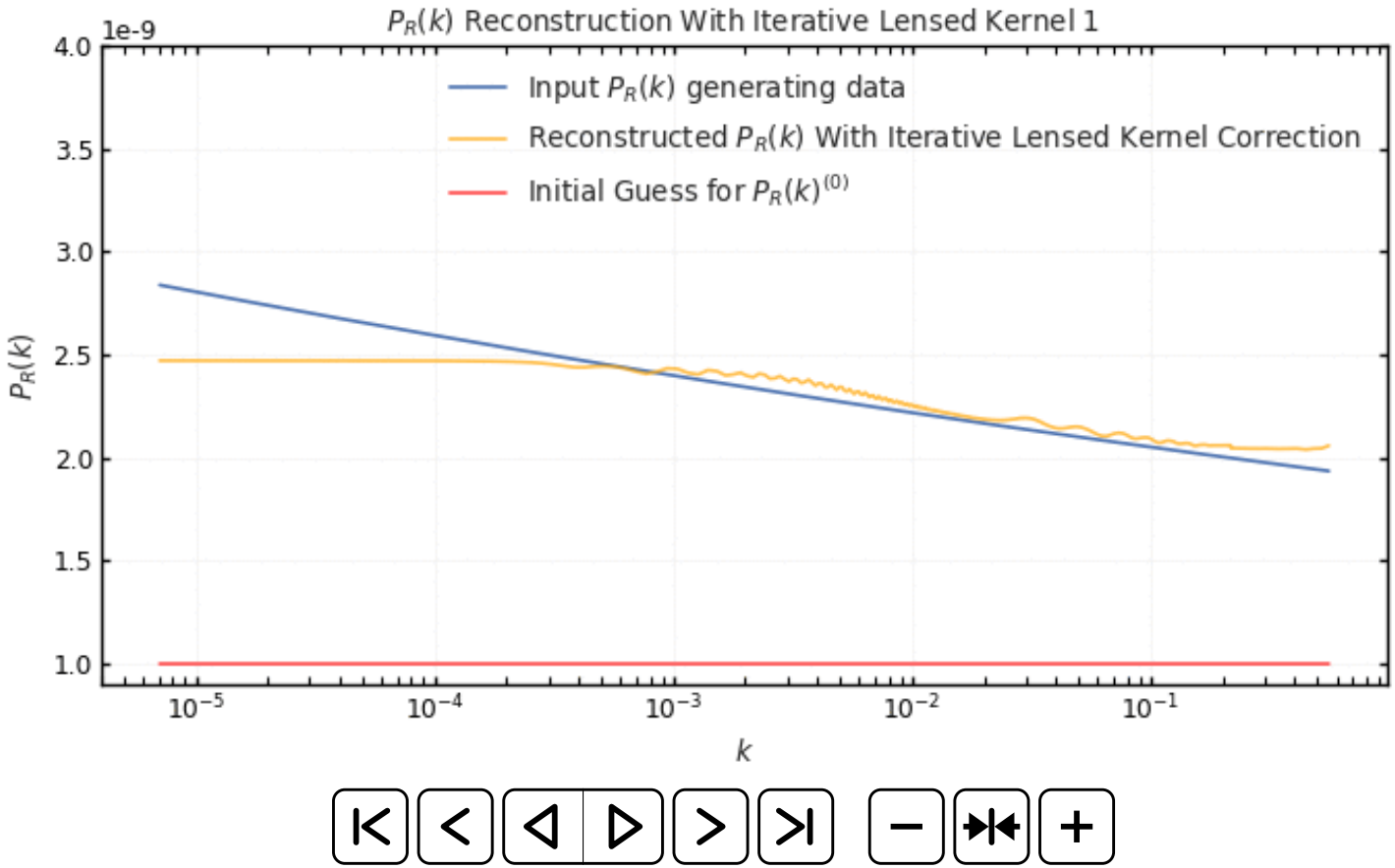

Power Law $P_R(k)$ Reconstruction on Lensed $\tilde{C}_L^{TT}$

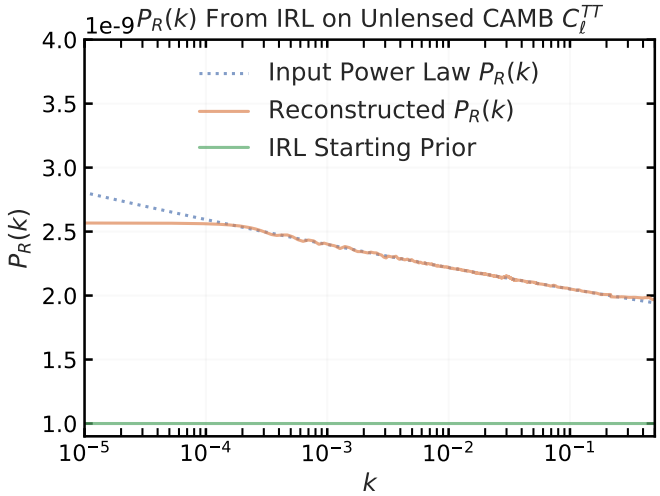

(a) Reference $P_R(k)$ from C_L^{TT} using RL

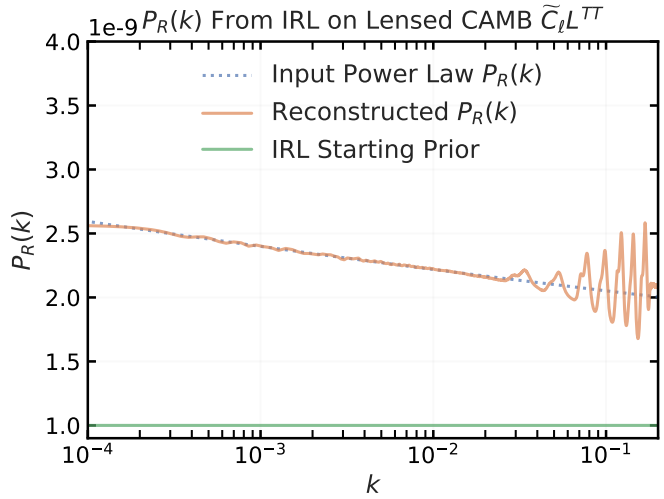

(b) $P_R(k)$ from $\tilde{C}_L^{TT}$ using RL

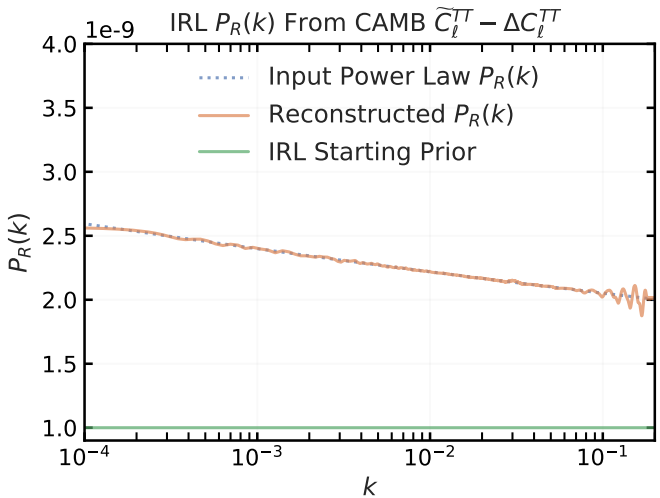

(c) $P_R(k)$ from $\tilde{C}_L^{TT}$ using RL + Template

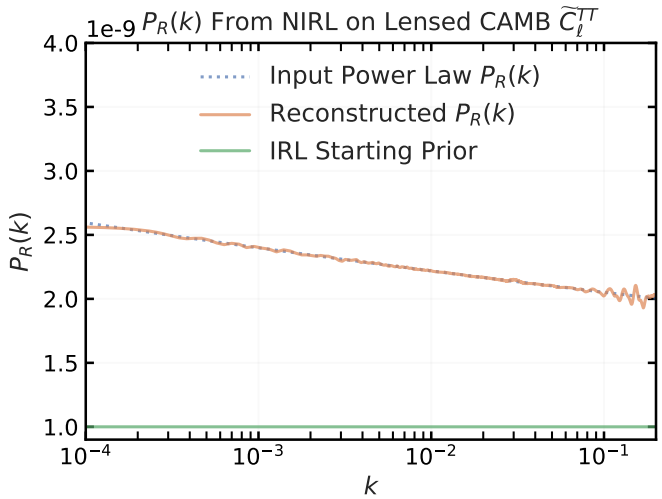

(d) $P_R(k)$ from $\tilde{C}_L^{TT}$ using NIRL

Power Law $P_R(k)$ Reconstruction on Lensed $\tilde{C}_L^{TT}$ Relative Error

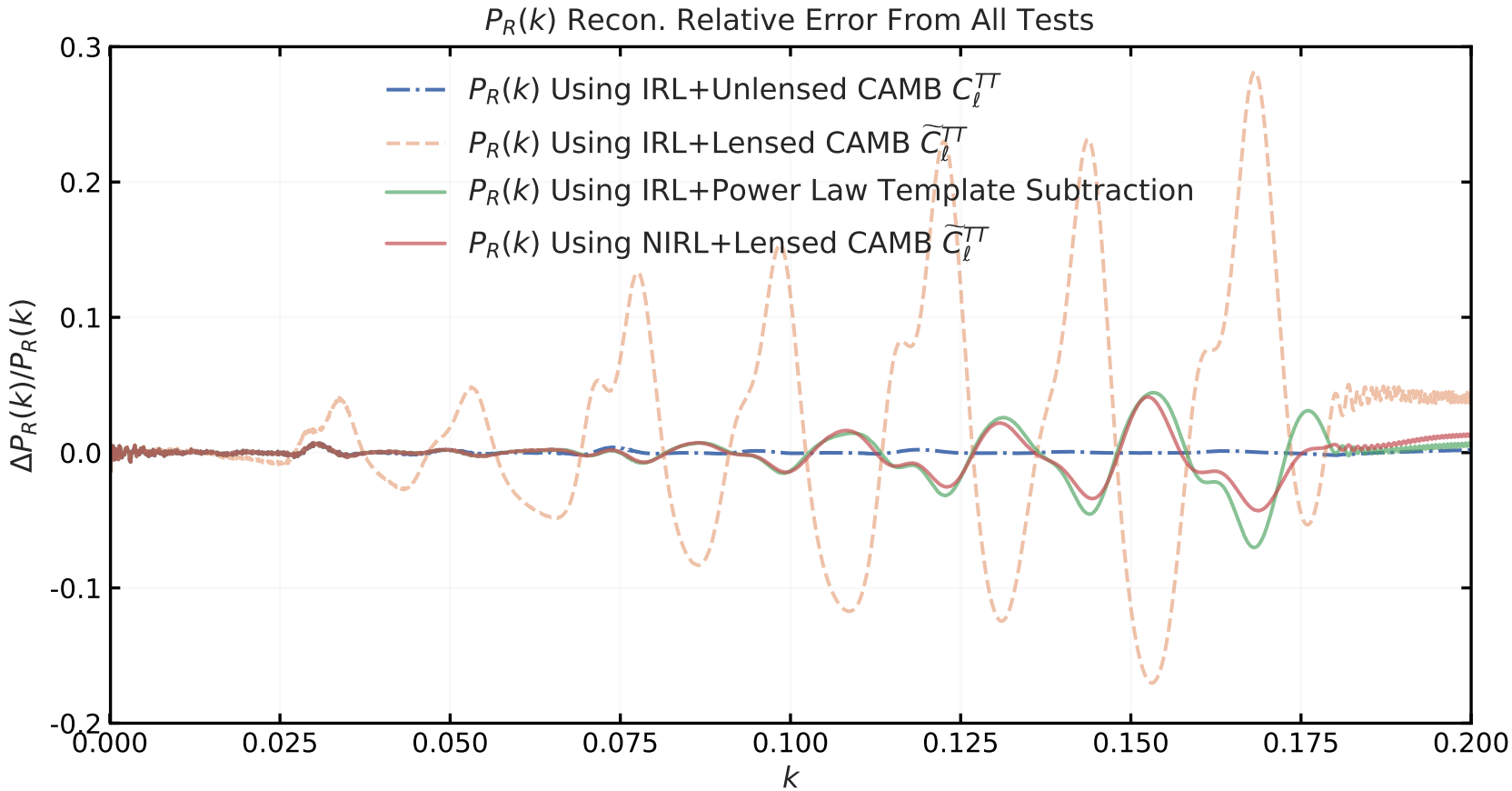

Figure 33: The figure displays the relative error of the 4 $P_R(k)$ reconstructions from the previous figures, with respect to first reconstruction.

Chandra and Souradeep, arXiv:2112.14008

Feature Based $P_R(k)$ Based Lensed $\tilde{C}_L^{TT}$ Data

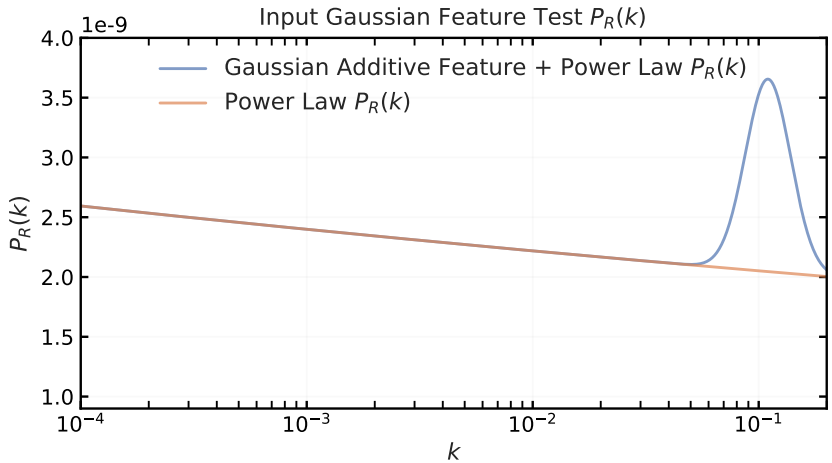

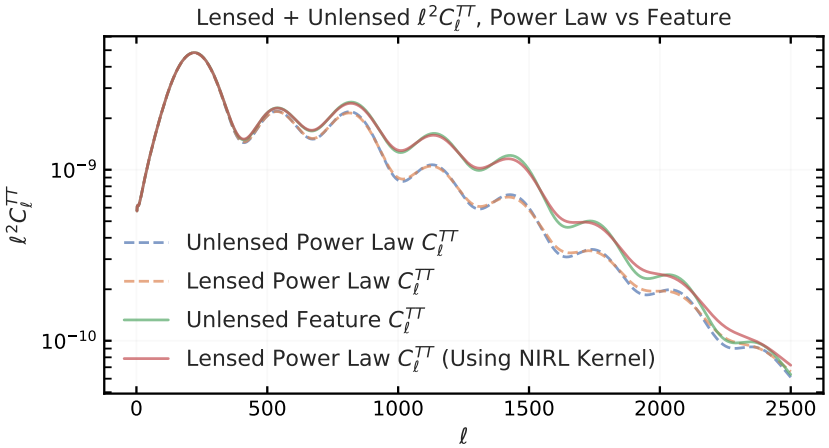

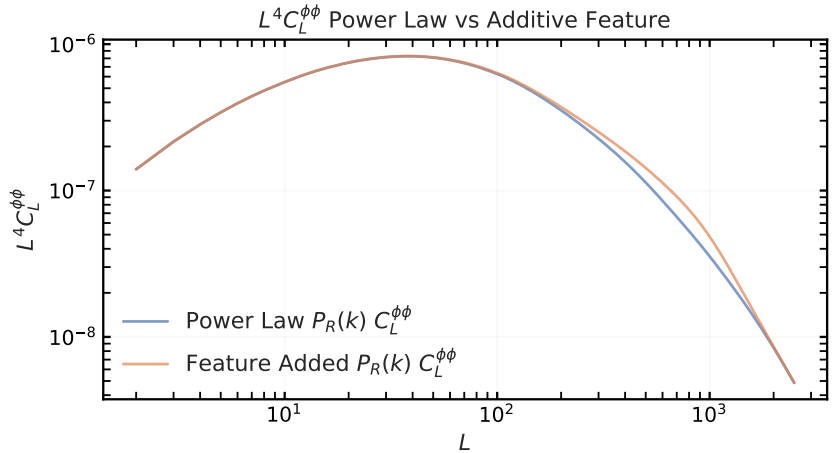

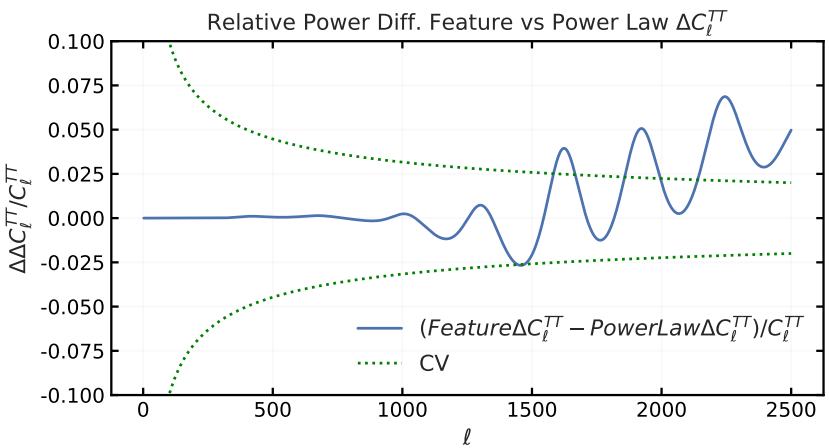

Feature Based $P_R(k)$ Reconstruction on Lensed $\tilde{C}_L^{TT}$

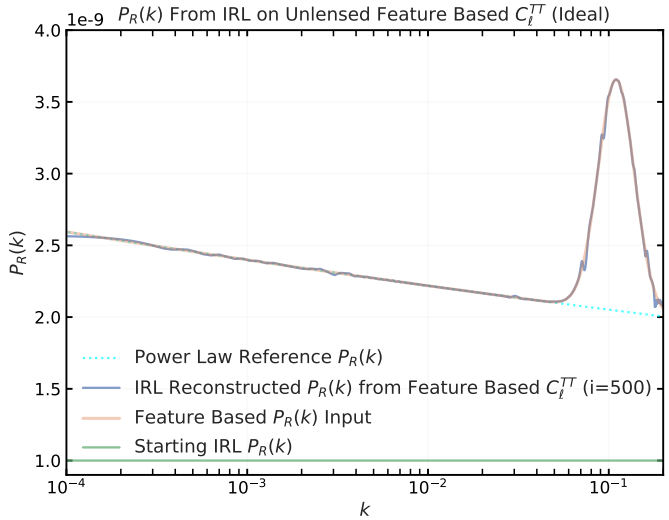

(a) Reference $P_R(k)$ from C_L^{TT} using RL

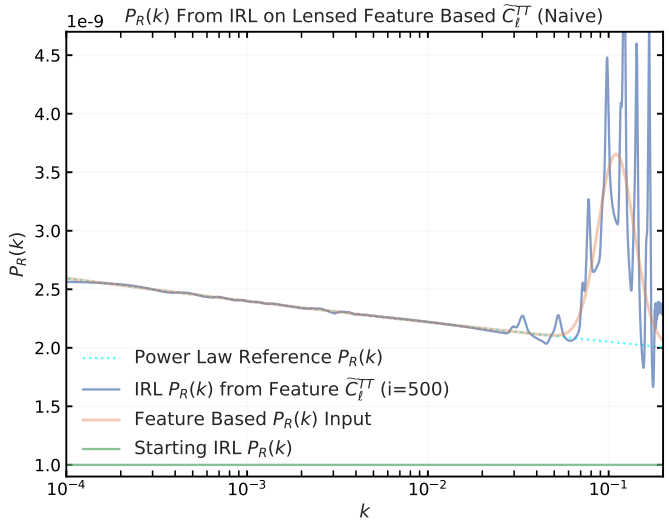

(b) $P_R(k)$ from $\tilde{C}_L^{TT}$ using RL

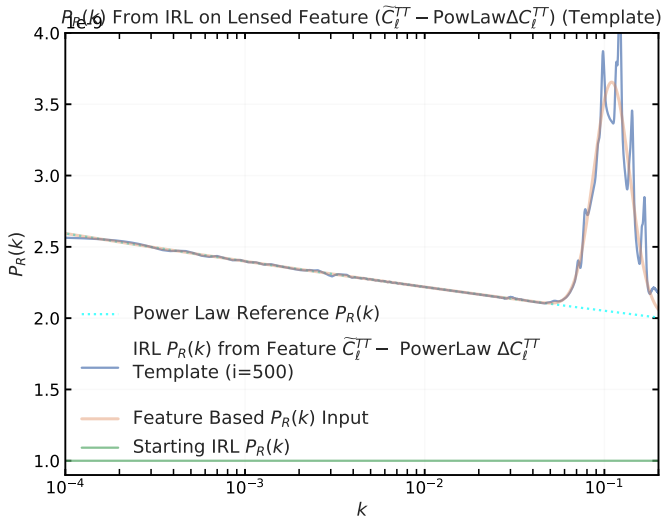

(c) $P_R(k)$ from $\tilde{C}_L^{TT}$ using RL + Template

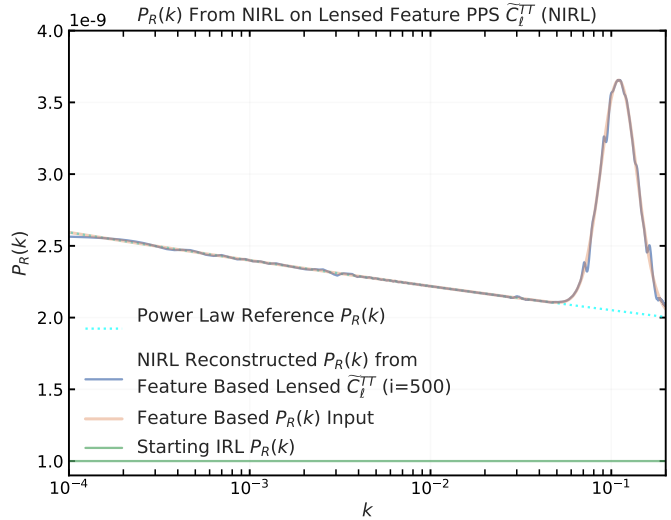

(d) $P_R(k)$ from $\tilde{C}_L^{TT}$ using NIRL

Feature Based $P_R(k)$ Reconstruction on Lensed $\tilde{C}_L^{TT}$ Relative Error

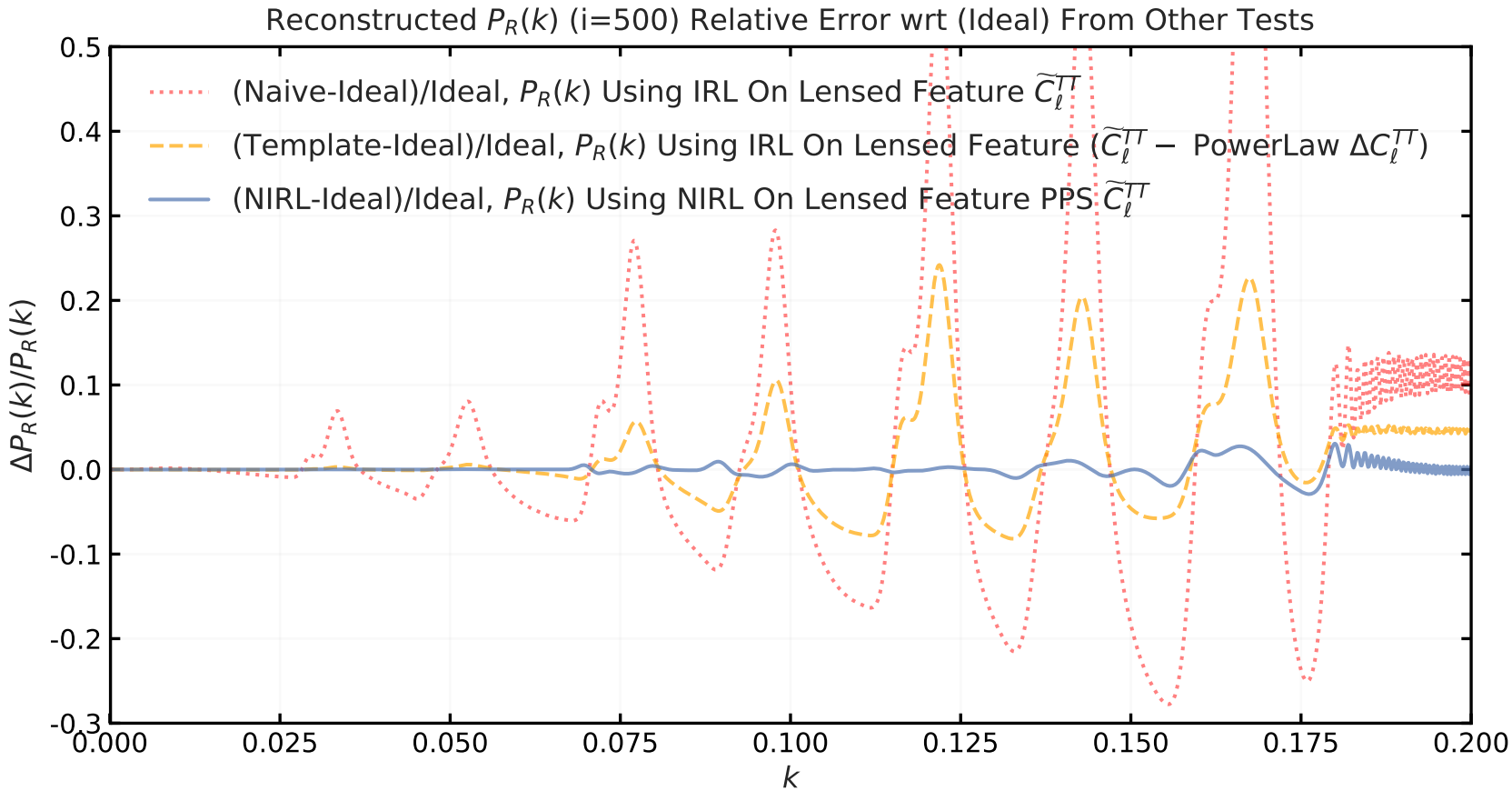

Figure 37: The figure displays the relative error of the 4 $P_R(k)$ reconstructions from the previous figures, with respect to first reconstruction.

Chandra and Souradeep, arXiv:2112.14008

Feature Based $P_R(k)$ Reconstruction on Lensed $\tilde{C}_L^{TT}$: Cosmic Variance Noise Limit

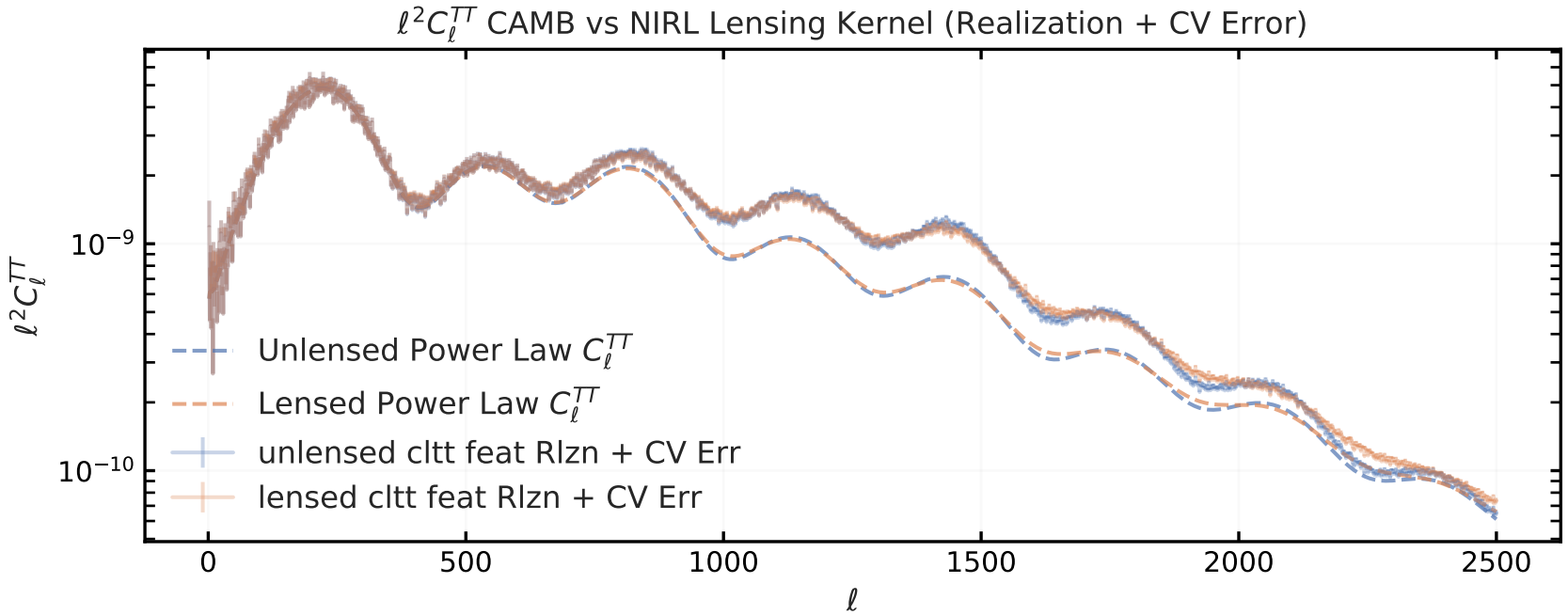

(a)

Figure 38: This plot shows the lensed and unlensed C_ℓ^{TT} using the Gaussian bump feature, in solid lines, generated as a realization based on cosmic variance error bars. It also shows the power law version, without any error bars or realization noise, in dashed lines.

Chandra and Souradeep, arXiv:2112.14008

Feature Based $P_R(k)$ Reconstruction on Lensed $\tilde{C}_L^{TT}$

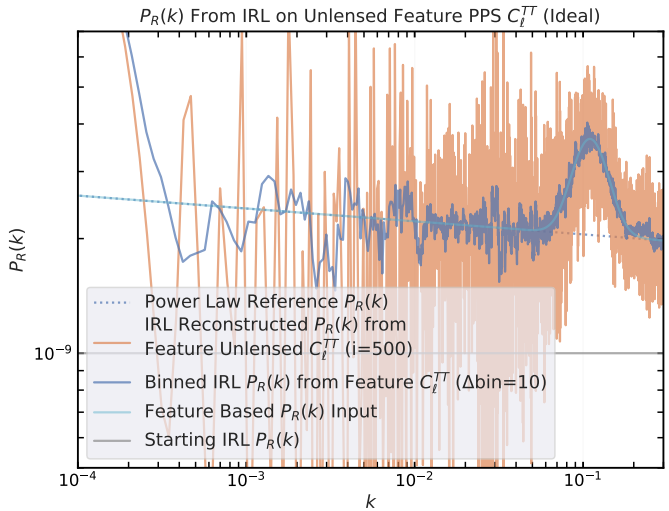

(a) $P_R(k)$ from C_L^{TT} using RL

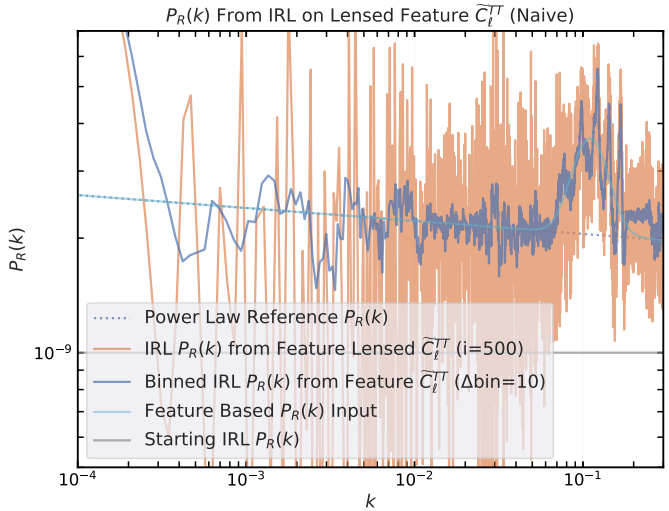

(b) $P_R(k)$ from $\tilde{C}_L^{TT}$ using RL

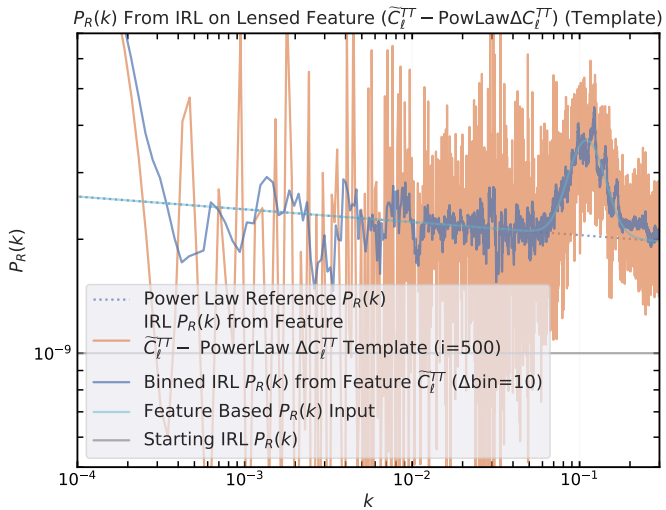

(c) $P_R(k)$ from $\tilde{C}_L^{TT}$ using RL + Template

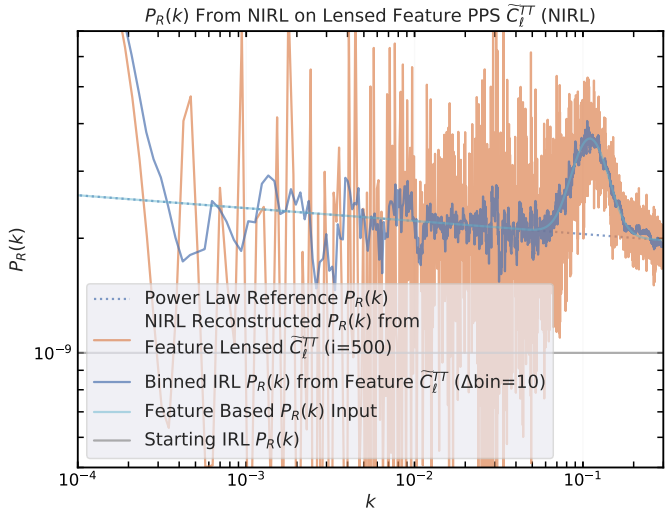

(d) $P_R(k)$ from $\tilde{C}_L^{TT}$ using NIRL

Feature Based $P_R(k)$ Reconstruction on Lensed $\tilde{C}_L^{TT}$ with CV Noise: Relative Error

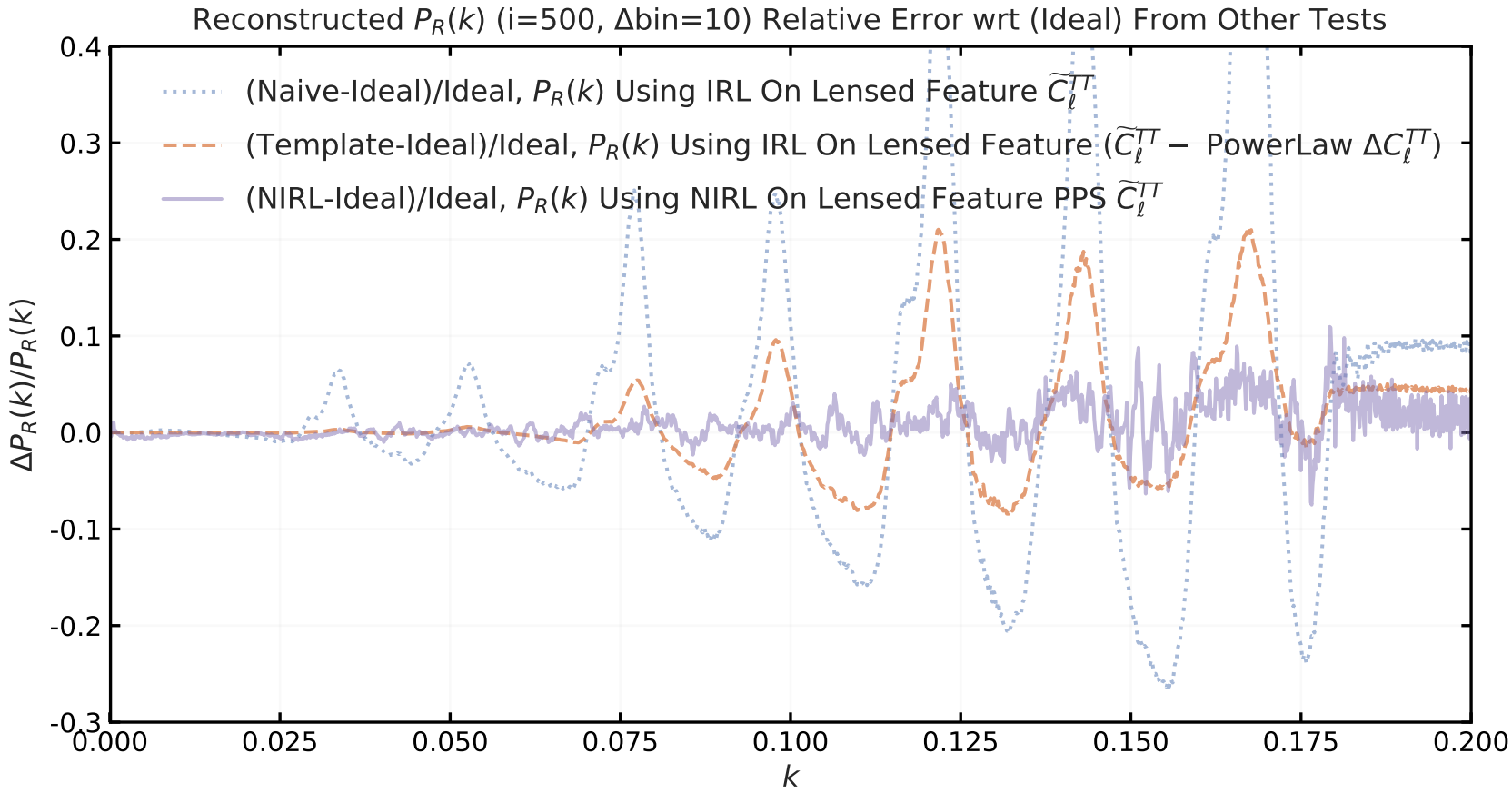

Figure 40: This figure shows the relative error of the 3 reconstructions of the $P_R(k)$ displayed in the previous plots, respectively, relative to the first reconstruction, which is held as the ideal reference reconstruction. These are based on 500 iterations of the RL algorithm.

Oscillatory Feature Based $P_R(k)$ Based Lensed $\tilde{C}_L^{TT}$ Data

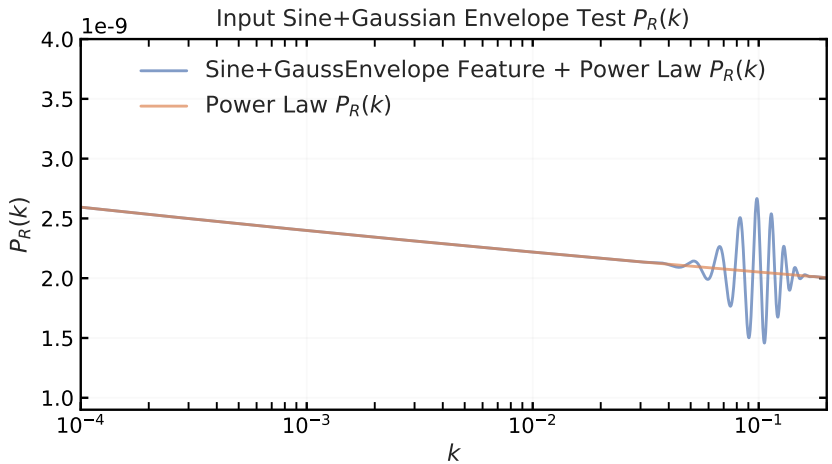

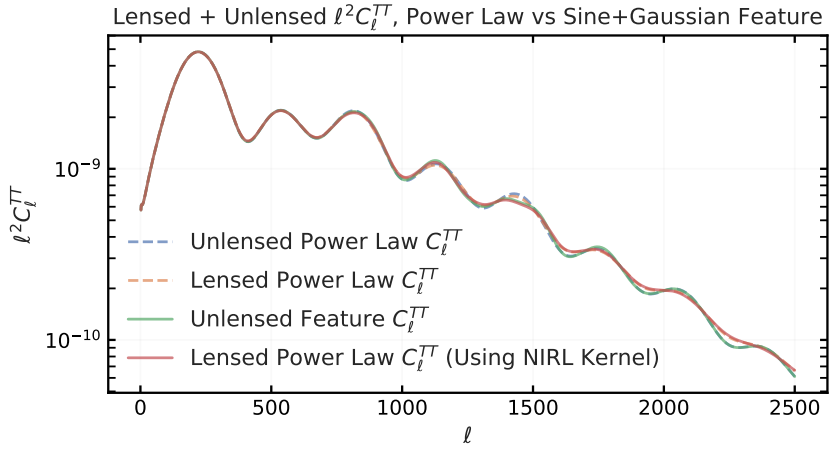

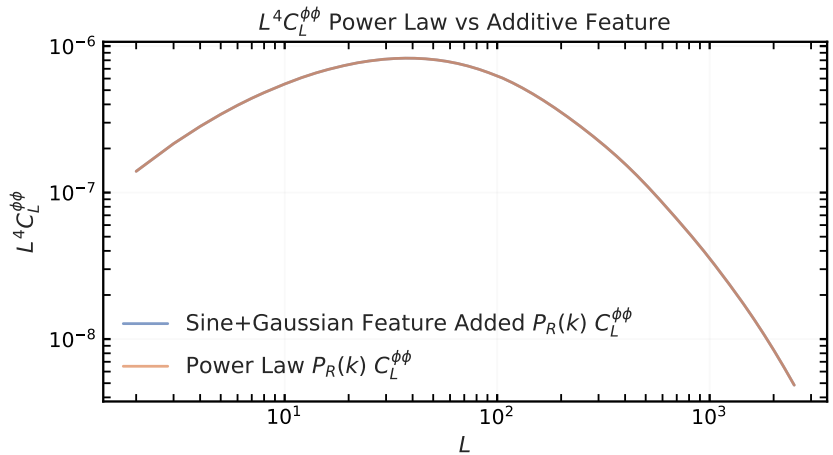

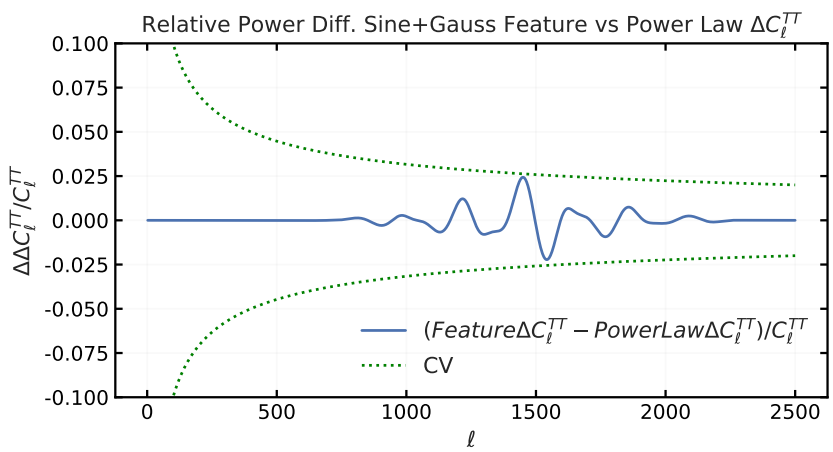

Oscillatory Feature $P_R(k)$ Reconstruction on Lensed $\tilde{C}_L^{TT}$

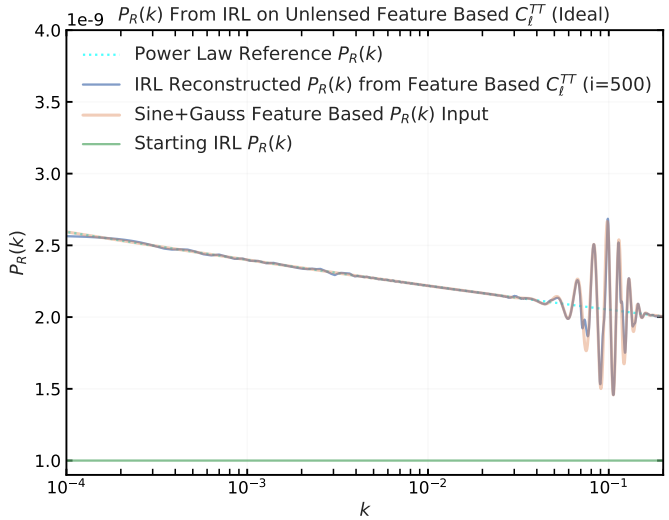

(a) Reference $P_R(k)$ from C_L^{TT} using RL

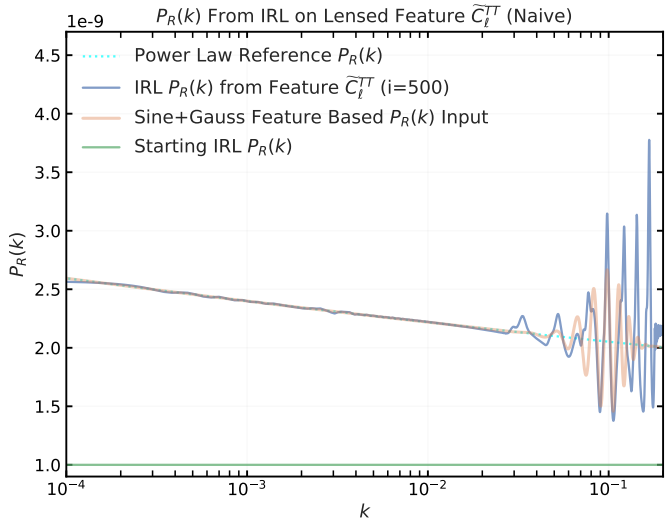

(b) $P_R(k)$ from $\tilde{C}_L^{TT}$ using RL

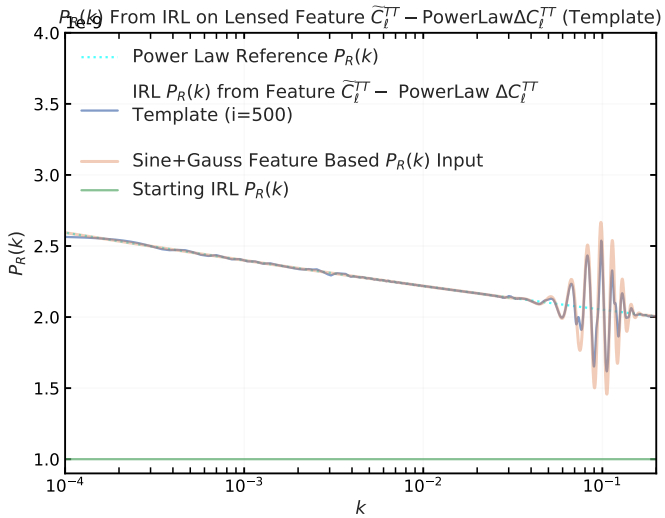

(c) $P_R(k)$ from $\tilde{C}_L^{TT}$ using RL + Template

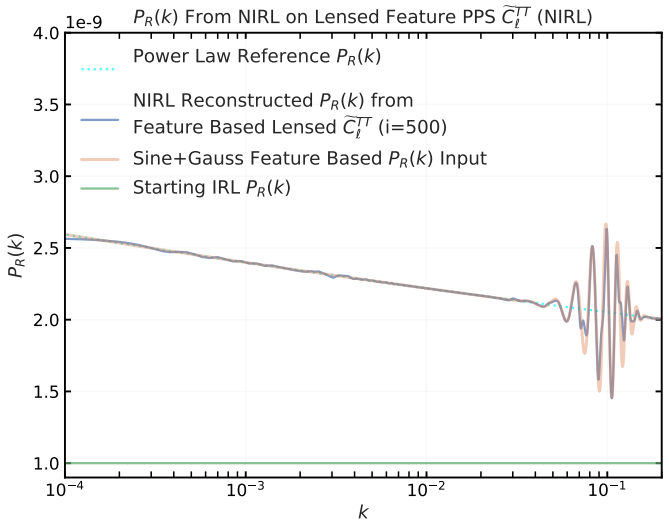

(d) $P_R(k)$ from $\tilde{C}_L^{TT}$ using NIRL

Oscillatory Feature Based $P_R(k)$ Reconstruction on Lensed $\tilde{C}_L^{TT}$ Relative Error

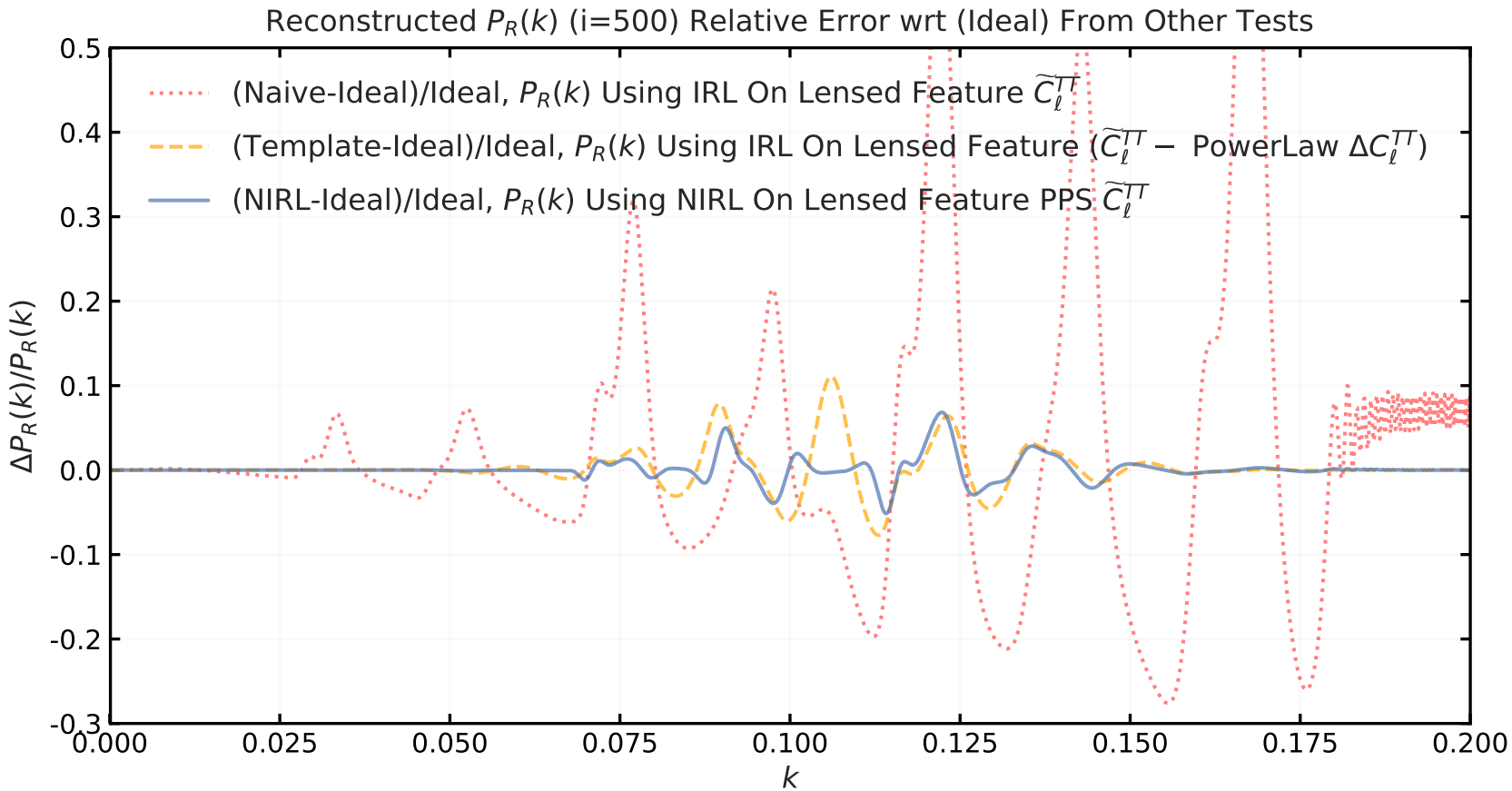

Figure 45: The figure displays the relative error of the 4 $P_R(k)$ reconstructions from the previous figures, with respect to first reconstruction.

Chandra and Souradeep, arXiv:2112.14008

Gravitational Lensing in Cosmology

Projected Weak Lensing Map,
Power Spectrum

?

Observed Temperature Anisotropy Map,
Power Spectrum,
(Lensed)

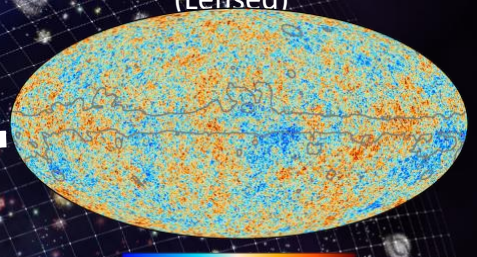

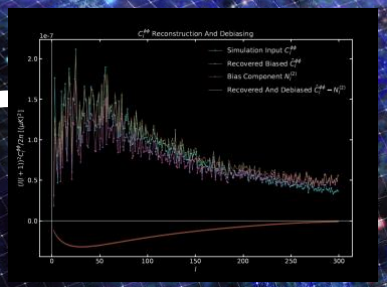

Inflation,
Primordial Scalar Perturbations

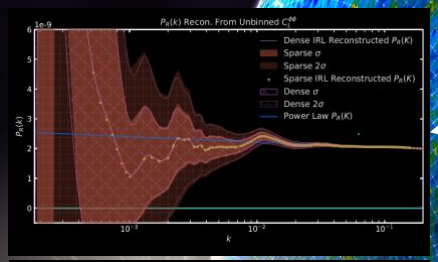

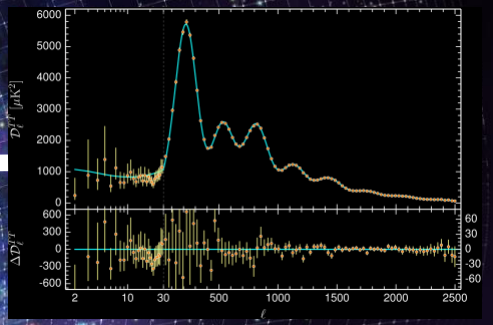

Primary Temperature Anisotropy Map,
Power Spectrum,
(Unlensed)

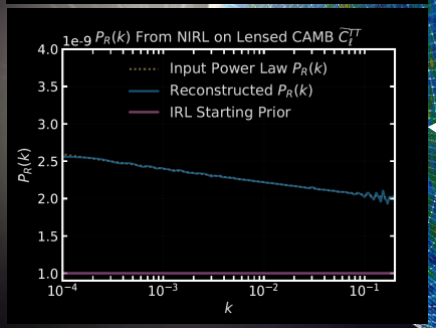

?

?

New Tools Developed :

1) RL + KSS
2) NIRL
3) ? Iterative QMVE ?

Chandra and Souradeep, JCAP10(2021)081
Chandra and Souradeep, arXiv:2112.14008

Why Use These Methods ?

- Planck and CORE proposal motivate the use of N-point interpolating logarithmic spline reconstruction, where each knot N is a free parameter. Broad spectrum model testing.
- RL is versatile, optimized for power spectra and model independent analysis. Reduces need for model fitting, while searching for novel features.
- NIRL is a simple, intuitive way to perform delensing in tandem with $P_R(k)$ reconstruction given ΛCDM kernel. Hardens against lensing caused biasing.

Challenges Addressed In This Work

- $P_R(k)$ from C_L^{TT} is in reality obtained from lensed $\tilde{C}_L^{TT}$. Earlier power law template subtraction is optimal for WMAP data. Planck Data shows lensing is a contaminant at high precision, high k region, needs consistent cleaning without any assumption of template, to avoid biasing real features. Can we do blind delensing of $\tilde{C}_L^{TT}$ to get true free-form $P_R(k)$?
- NIRL provides a simple, intuitive way to delens $\tilde{C}_L^{TT}$ while keeping $P_R(k)$ deconvolution consistently free-form and unbiased.
- NIRL has algorithmic utility beyond CMB, any deconvolution involving positive definite quantities, order of magnitude weak convolution signal, can utilize it.

Possible Future Work On This Topic

- Implement NIRL reconstruction formalism on Planck mission data $\tilde{C}_L^{TT}$ to reconstruct free form $P_R(k)$ with unbiased consistency.
- Implement the KSS algorithm from Chandra and Souradeep, JCAP10(2021)081, to NIRL for a full covariance matrix analysis of the $P_R(k)$ reconstruction.
- Prepare a reconstruction package for incoming CMB data from Simons Observatory and CMB-Stage 4, both of which have a key focus on Inflation and primordial physics.

CORE Forecasts

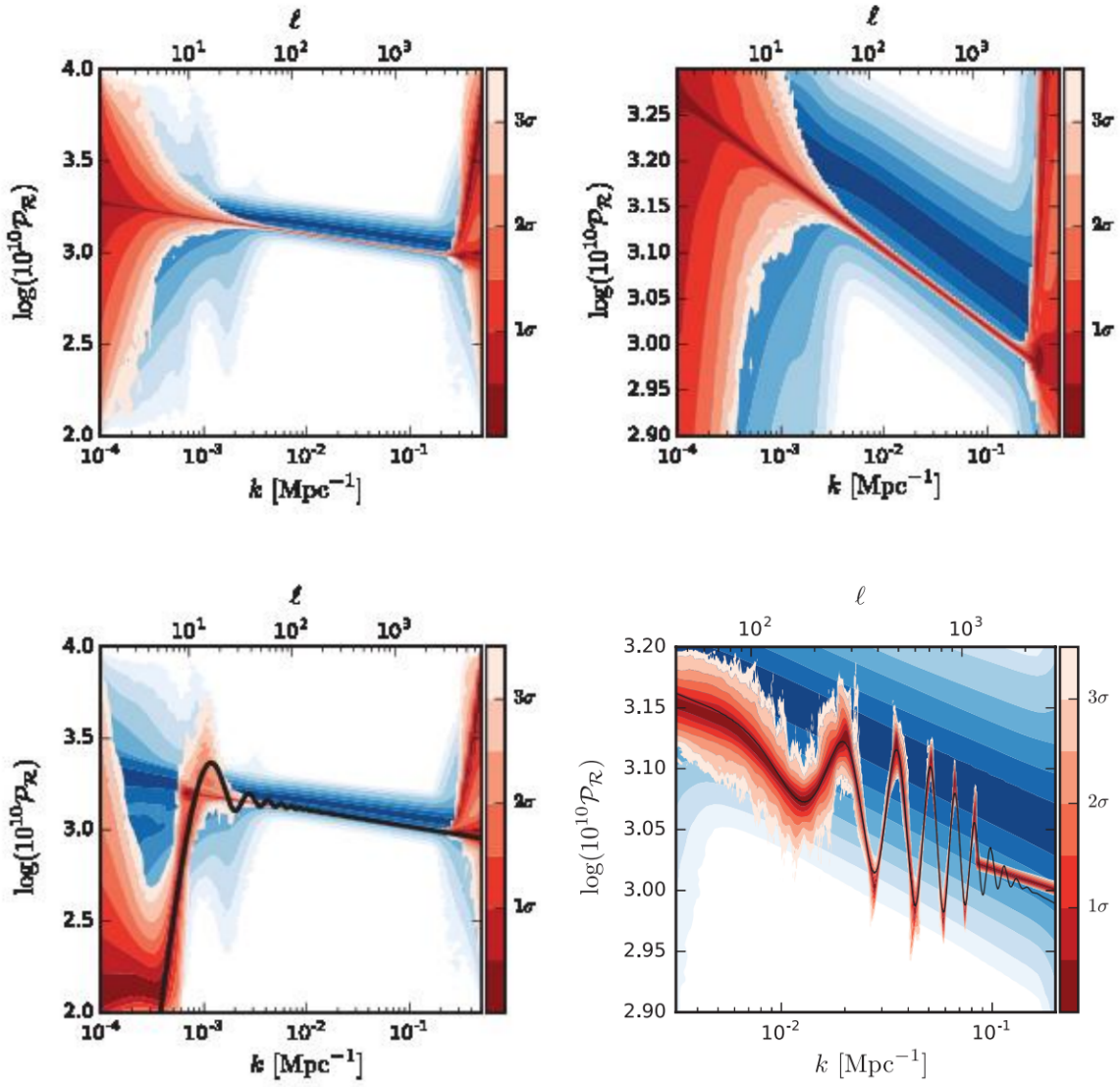

Cosmic ORigins Explorer proposed $P_R(k)$ reconstructions (Red) and precision compared to Planck (Blue), for both power law model and feature producing modified inflation models.

Fin

Weak Lensing Representation in Spherical Harmonic Basis

We need an appropriate mathematical basis to express the lensing statistics in. We use the spherical harmonic basis for the full sky calculations.

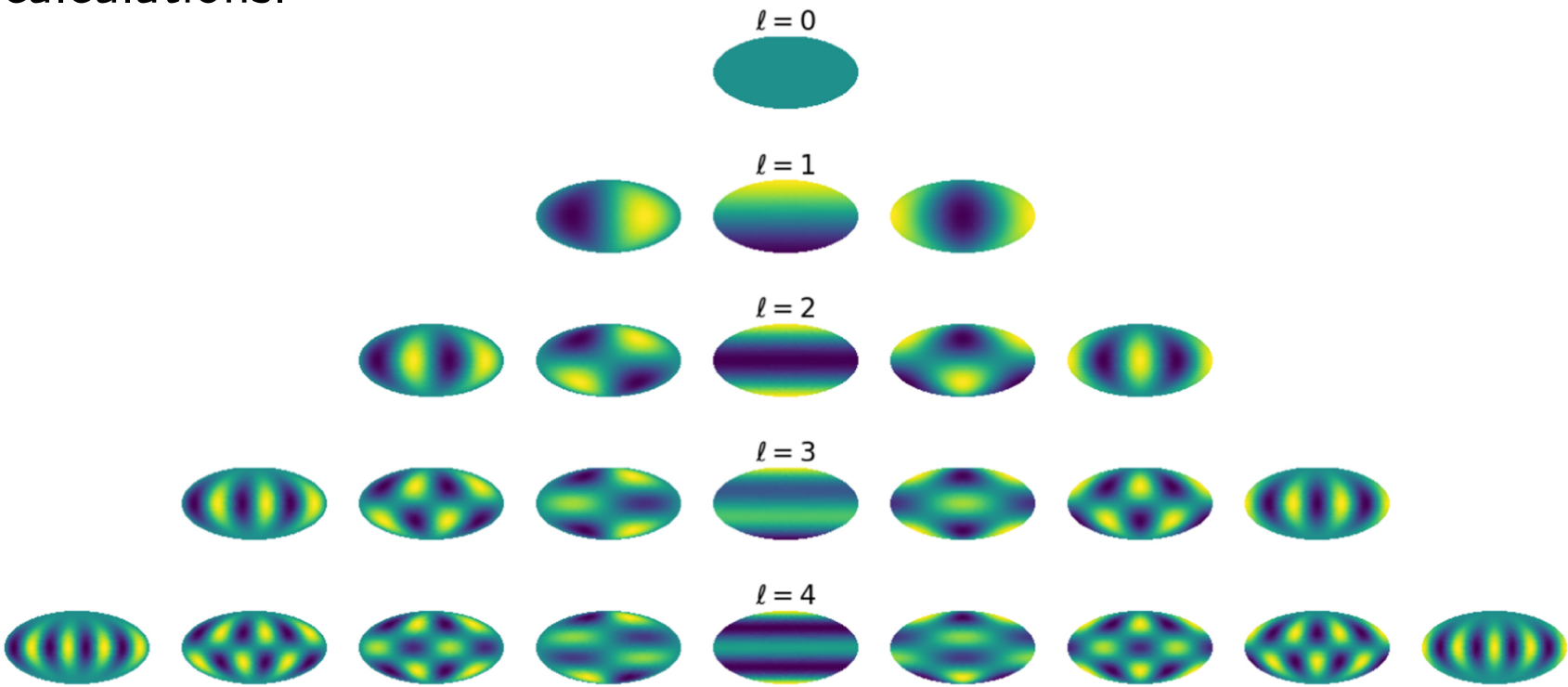

Figure 50: Spherical harmonics in Mollweide projection, Cunningham et al. (Quantifying the Stellar Halo's Response to the LMC's Infall with Spherical Harmonics)

Weak Lensing Statistics in Spherical Harmonic Basis

We decompose the temperature anisotropy map in spherical harmonic basis

$$\phi(\hat{\mathbf{n}}) = \sum_{LM} \phi_{LM} Y_{LM}(\hat{\mathbf{n}}) \tag{20}$$

$$T(\hat{\mathbf{n}}) = \sum_{LM} \Theta_{LM} Y_{LM}(\hat{\mathbf{n}}) \tag{21}$$

We can study the statistical properties of a given random field by the 2-point correlation function of the harmonic coefficients, which gives the covariance matrix

$$cov(\Theta_{l_1 m_1} \Theta_{l_2 m_2}) = \langle \Theta_{l_1 m_1} \Theta_{l_2 m_2} \rangle - \langle \Theta_{l_1 m_1} \rangle \langle \Theta_{l_2 m_2} \rangle \tag{22}$$

Where $\langle\rangle$ is the expectation value.

Statistical Assumptions About Weak Lensing and CMB

Under the framework of the ΛCDM standard model we can assume

- Underlying unlensed temperature anisotropy field Θ_{LM} to be Statistically Isotropic and Gaussian

$$\langle \Theta_{LM} \Theta^*_{L'M'} \rangle = C_L^{TT} \delta_{LL'} \delta_{MM'} \tag{23}$$

- Weak lensing potential field ϕ_{LM} to be Statistically Isotropic and Gaussian

$$\langle \phi_{LM} \phi^*_{L'M'} \rangle = C_L^{\phi\phi} \delta_{LL'} \delta_{MM'} \tag{24}$$

Weak Lensing induces statistical anisotropy in the temperature field.

Biposh Representation Of Covariance Matrix

We can better represent the 2-point correlation function in the Bipolar Spherical Harmonic basis as it naturally incorporates the off diagonal components of the covariance matrix.

$$\mathcal{A}^{LM}_{ll'} = \sum_{mm'} \langle a_{lm} a^*_{l'm'} \rangle (-1)^{m'} \mathcal{C}^{LM}_{lml'-m'} \tag{25}$$

Where the general 2-point function in the Biposh coefficients are given by

$$C(\hat{n}, \hat{n}') = \sum_{ll'} \sum_{LM} \mathcal{A}^{LM}_{ll'} \{ Y_l(\hat{n}) \otimes Y_{l'}(\hat{n}') \}_{LM} \tag{26}$$

(Hajian and Souradeep (2003), Souradeep et al. (2006))

CMB Weak Lensing Quadratic Estimator

Following the formalism developed by Hu (2001), Okamoto and Hu (2003) and D Hanson et al. (2011), we rederive in the Biposh formalism.

$$\mathcal{A}^{LM}_{ll'}|_{obs} = \mathcal{A}^{LM}_{ll'}|_{S.I.} + \mathcal{A}^{LM}_{ll'}|_{\phi} \tag{27}$$

$$\begin{aligned} \langle \mathcal{A}^{LM}_{ll'}|_{S.I.} \rangle &= (-1)^{l} C_l^{TT} \sqrt{2l+1}\delta_{L0} \\ \langle \mathcal{A}^{LM}_{ll'}|_{\phi} \rangle &= \frac{(-1)^L}{\sqrt{2L+1}} \phi_{LM} \left[C_{l'}^{TT} F_{lLl'} + C_l^{TT} F_{l'Ll} \right] \end{aligned} \tag{28}$$

$$\begin{aligned} F_{l_1 l_2 l_3} &= \frac{1}{2}[l_2(l_2+1) + l_3(l_3+1) - l_1(l_1+1)] \\ &\sqrt{\frac{(2l_1+1)(2l_2+1)(2l_3+1)}{4\pi}} \begin{pmatrix} l_1 & l_2 & l_3 \\ 0 & 0 & 0 \end{pmatrix} \\ &\forall (l_1 + l_2 + l_3) = \text{even} \end{aligned} \tag{29}$$

Minimum Variance Quadratic Estimator In Biposh Formalism

$$\widehat{\phi}_{LM} = \sum_{ll'} w^L_{ll'} \frac{\mathcal{A}^{LM}_{ll'}|_{obs}}{\mathcal{K}^L_{ll'}|_\phi} \tag{30}$$

$$\langle \widehat{\phi}_{LM} \widehat{\phi}^*_{L_1 M_1} \rangle = \sum_{ll'} (w^L_{ll'})^2 \frac{2 C_l^{TT} C_{l'}^{TT}}{(\mathcal{K}^L_{ll'}|_\phi)^2} + \langle \phi_{LM} \phi^*_{L_1 M_1} \rangle \tag{31}$$

$$\widehat{C}^{\widehat{\phi}\widehat{\phi}}_L = N^{(0)}_L + C^{\phi\phi}_L$$

$$\sum_{ll'} w^L_{ll'} = 1 \tag{32}$$

Lagrange Function and method of Undetermined Multipliers,

$$\mathcal{L} = \sum_{ll'} (w^L_{ll'})^2 \frac{2 C_l^{TT} C_{l'}^{TT}}{(\mathcal{K}^L_{ll'}|_\phi)^2} - \lambda [\sum_{ll'} w^L_{ll'} - 1] \tag{33}$$

Minimum Variance Quadratic Estimator In Biposh Formalism

$$\widehat{\phi}_{LM} = \frac{1}{\left[\sum_{ll'} \frac{(\mathcal{K}^{L}_{ll'}|_{\phi})^2}{C_l^{TT} C_{l'}^{TT}}\right]} \sum_{ll'} \frac{\mathcal{K}^{L}_{ll'}|_{\phi}}{C_l^{TT} C_{l'}^{TT}} \widehat{\mathcal{A}}^{LM}_{ll'} \tag{34}$$

$$\widehat{C}_L^{\phi\phi} = N_L^{(0)} + C_L^{\phi\phi} + N_L^{(1)} + N_L^{(2)} \tag{35}$$

$$N_L^{(0)} = \frac{2}{\left[\sum_{ll'} \frac{(\mathcal{K}^{L}_{ll'}|_{\phi})^2}{C_l^{TT} C_{l'}^{TT}}\right]} \tag{36}$$

Minimum Variance Quadratic Estimator Trispectra Biases

$$N_L^{(1)} = \frac{2}{\mathcal{W}_L^2} \sum_{l_1 l_2 l_3 l_4} (-1)^{l_2+l_3} \frac{\mathcal{K}^L_{l_1 l_2}|_\phi \mathcal{K}^L_{l_3 l_4}|_\phi}{C_{l_1}^{TT} C_{l_2}^{TT} C_{l_3}^{TT} C_{l_4}^{TT}} \sum_{L'} \left[\begin{Bmatrix} l_1 & l_2 & L \\ l_4 & l_3 & L' \end{Bmatrix} (2L'+1) C_{L'}^{\phi\phi} \mathcal{K}^{L'}_{l_1 l_3}|_\phi \mathcal{K}^{L'}_{l_2 l_4}|_\phi \right] \tag{37}$$

$$\begin{aligned} N_L^{(2)} =& 2C_L^{\phi\phi} \frac{(-1)^L}{\sqrt{2L+1}\mathcal{W}_L^2} \sum_{l_1 l_2} \frac{F_{l_2 L l_1} \mathcal{K}^L_{l_1 l_2}|_\phi}{C_{l_1}^{TT} C_{l_2}^{TT}} \\ & \left[\sum_{l_a l_b} C_{l_a}^{TT} C_{l_b}^{\phi\phi} F^2_{l_1 l_a l_b} \left(\frac{l_1(l_1+1) + l_a(l_a+1) - l_b(l_b+1)}{(2l_1+1) l_1(l_1+1)} \right) \right. \\ & \left. - 2R(l_1(l_1+1) - 1/3) C_{l_1}^{TT} \right] \left(\sum_{l_3 l_4} \frac{(\mathcal{K}^L_{l_3 l_4}|_\phi)^2}{C_{l_3}^{TT} C_{l_4}^{TT}} \right) \end{aligned} \tag{38}$$

MVQE Reconstruction of $C_L^{\kappa\kappa}$ With $N_L^{(2)}$ Debiasing

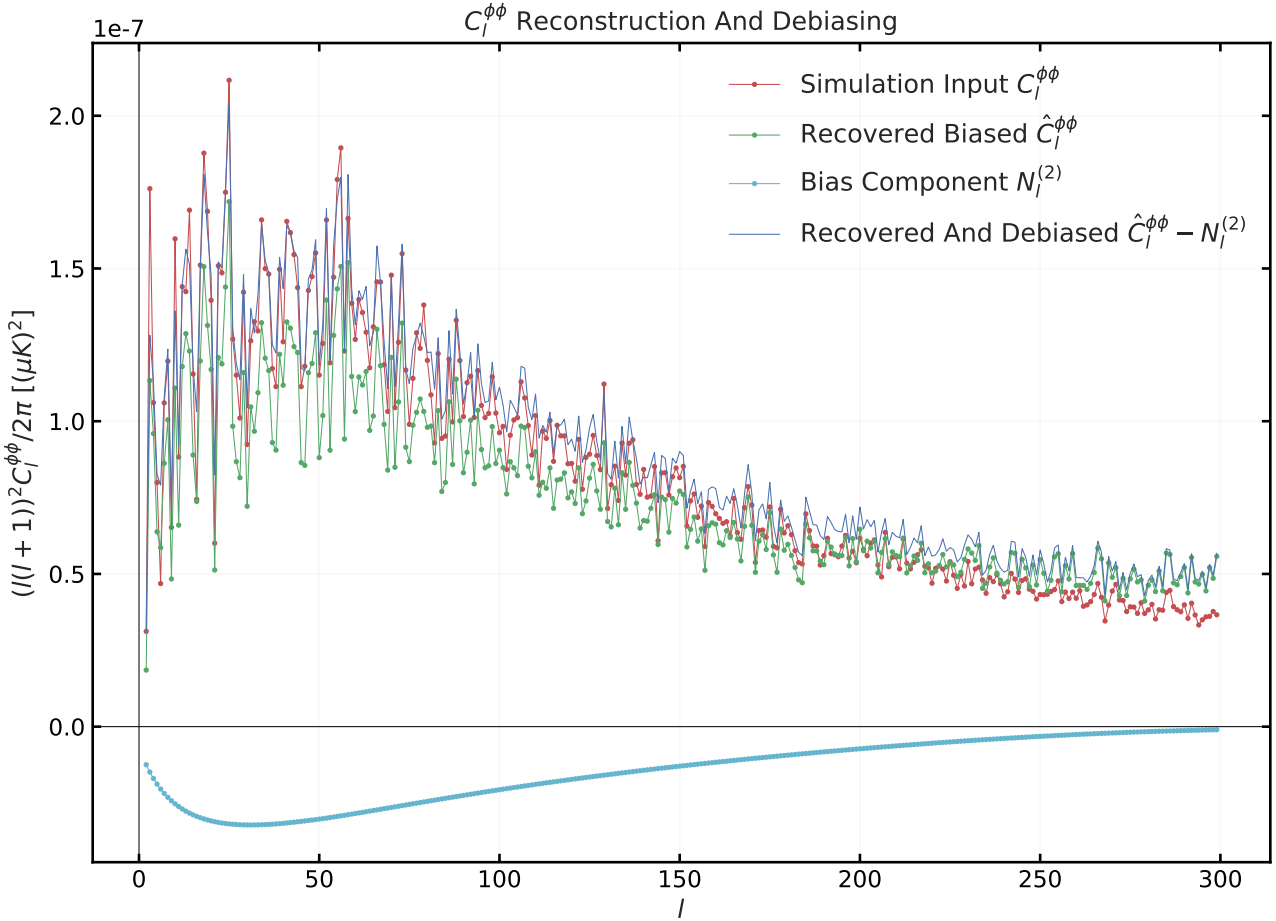

Figure 51: $C_L^{\kappa\kappa}$ reconstruction debiasing of $N_L^{(2)}$ component.

MVQE Reconstruction of $C_L^{\kappa\kappa}$ With $N_L^{(2)}$ Debiasing

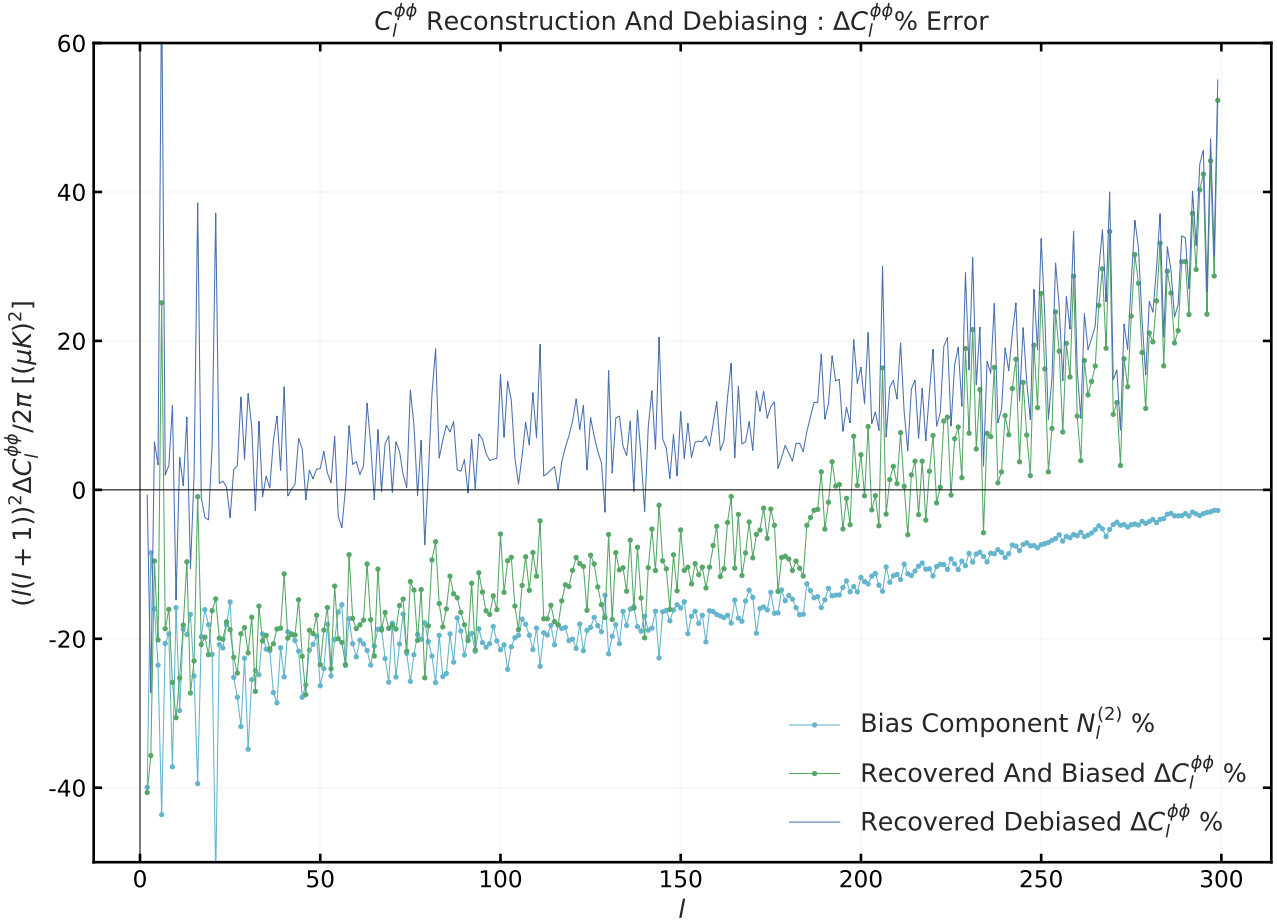

Figure 52: $N_L^{(2)}$ bias correction.

CMB Temperature Anisotropy Weak Lensing Formalism

The lensing remapping is expressed as

$$\tilde{\Theta}(\hat{n}) = \Theta(\hat{n} + \vec{\alpha}) \tag{39}$$

- Remapping angle vector can be expressed as gradient-scalar plus curl-vector

$$\vec{\alpha} = \nabla_{\hat{n}}\phi + \nabla_{\hat{n}} \times \Omega \tag{40}$$

- First order scalar metric perturbations only provide gradient type contribution
- For LSS induced lensing scalar metric perturbations relevant

Weiner Filtering ϕ Map

$$\widehat{\phi}_{LM} = \sum_{ll'} w^{L}_{ll'} \frac{\widehat{\mathcal{A}}^{LM}_{ll'}|_{S.I.}}{\mathcal{K}^{L}_{ll'}|_{\phi}} + \phi_{LM} \tag{41}$$

$$d = s + n, \quad \sigma_d^2 = \sigma_s^2 + \sigma_n^2, \quad p(s) \propto e^{-\frac{s^2}{2\sigma_s^2}}, \quad p(n) \propto e^{-\frac{n^2}{2\sigma_n^2}} \tag{42}$$

$$P(s|d) = \frac{P(d|s)P(s)}{P(d)}, \quad P(d|s) \propto e^{-\frac{(d-s)^2}{2\sigma_n^2}}, P(s|d) \propto e^{-\frac{1}{2}\left[\frac{(d-s)^2}{\sigma_n^2} + \frac{s^2}{\sigma_s^2}\right]} \tag{43}$$

$$\frac{\partial p(s|d)}{\partial s} = \frac{2(d-s)}{\sigma_n^2} + \frac{2s}{\sigma_s^2} = 0, \quad s = \frac{\sigma_s^2}{\sigma_s^2 + \sigma_n^2} d \tag{44}$$

$$\phi^{(W.F.)}_{LM} = \frac{C_L^{\phi\phi}}{C_L^{\phi\phi} + N_L} \hat{\phi}_{LM} \tag{45}$$

$$\mathcal{R}_{\mathbf{k}} = \Psi_{\mathbf{k}} + H\frac{\delta\varphi_{\mathbf{k}}}{\dot{\varphi}} \tag{46}$$

$$S = \int d^4x\sqrt{-g}\Big[-\frac{1}{2}\partial_\mu\varphi\partial^\mu\varphi - V(\varphi)\Big] \tag{47}$$

$$\varphi(\mathbf{x}, t) = \varphi(t) + \delta\varphi(\mathbf{x}, t) \tag{48}$$

$$\dot{\varphi}^2 << V(\varphi) \tag{49}$$

$$R_{\mu\nu} - \frac{1}{2}g_{\mu\nu}R = 8\pi G_N T_{\mu\nu} \tag{50}$$

$$\mathcal{P}_{\mathcal{R}}(k) = A_s\left(\frac{k}{k_*}\right)^{n_s-1} \tag{51}$$

$$C_L^{TT} = \int d(\ln k)\mathcal{P}_{\mathcal{R}}(k)|\,T_L^{(S)}(k)|^2 \tag{52}$$

$$\Theta(\hat{\mathbf{n}}) = \frac{\Delta T(\hat{\mathbf{n}})}{T_o} \tag{53}$$

$$C_L^{\phi\phi} = 4\pi \int P_R(k)\Big[\int_0^{\chi_*} 2T_\phi(k;\eta_0-\chi)\Big(\frac{(\chi_*-\chi)}{\chi_*\chi}\Big)j_L(k\chi)d\chi\Big]^2\frac{dk}{k} \tag{54}$$

$$\phi(\hat{n}) = -2\int_0^{\chi_*} \Phi(\chi\hat{n};\eta_0-\chi)\frac{(\chi_*-\chi)}{(\chi_*\chi)}d\chi \tag{55}$$

$$\Phi(\mathbf{k};\eta) = T_\Phi(k;\eta)\mathcal{R}(k). \tag{56}$$

$$\widetilde{\Theta}(\hat{\mathbf{n}}) = \Theta(\hat{\mathbf{n}}') = \Theta(\hat{\mathbf{n}} + \vec{\nabla}\phi(\hat{\mathbf{n}})). \tag{57}$$

$$\widetilde{C}_l^{TT} = C_l^{TT} + C_l^{TT} \sum_{l_1} C_{l_1}^{\phi\phi} S_{ll_1}^{(b)} + \sum_{l_1 l_2} C_{l_1}^{\phi\phi} C_{l_2}^{TT} S_{ll_1 l_2}^{(a)} \tag{58}$$

Reconstruction Initial Guess Sensitivity

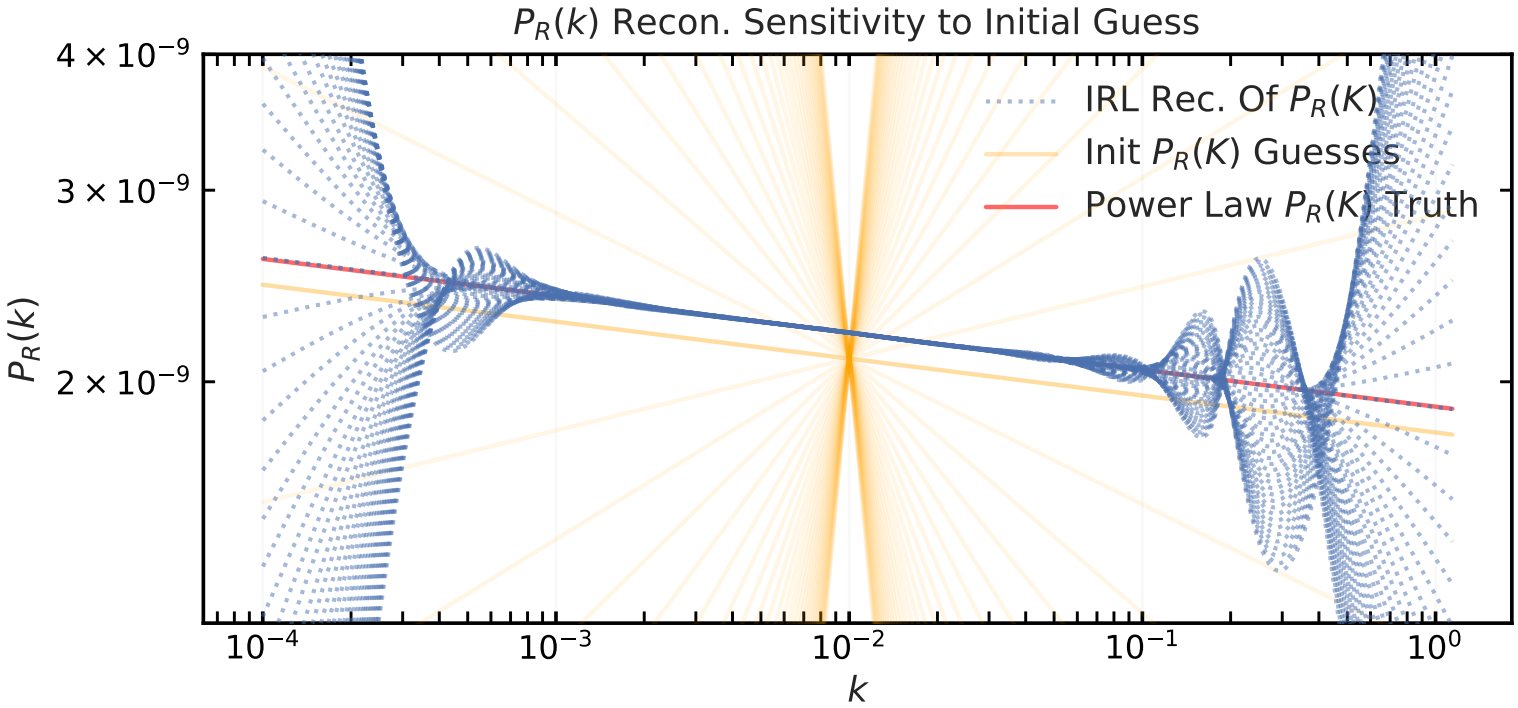

(a)

Figure 53: Figure a) shows the reconstructed $P_R(k)$ in blue dashed lines, given different initial guesses $P_R(k)^{(i=0)}$ in yellow lines varying by slope n_s. The red lines shows the original injected power spectrum $P_R(K)$.

Kernel

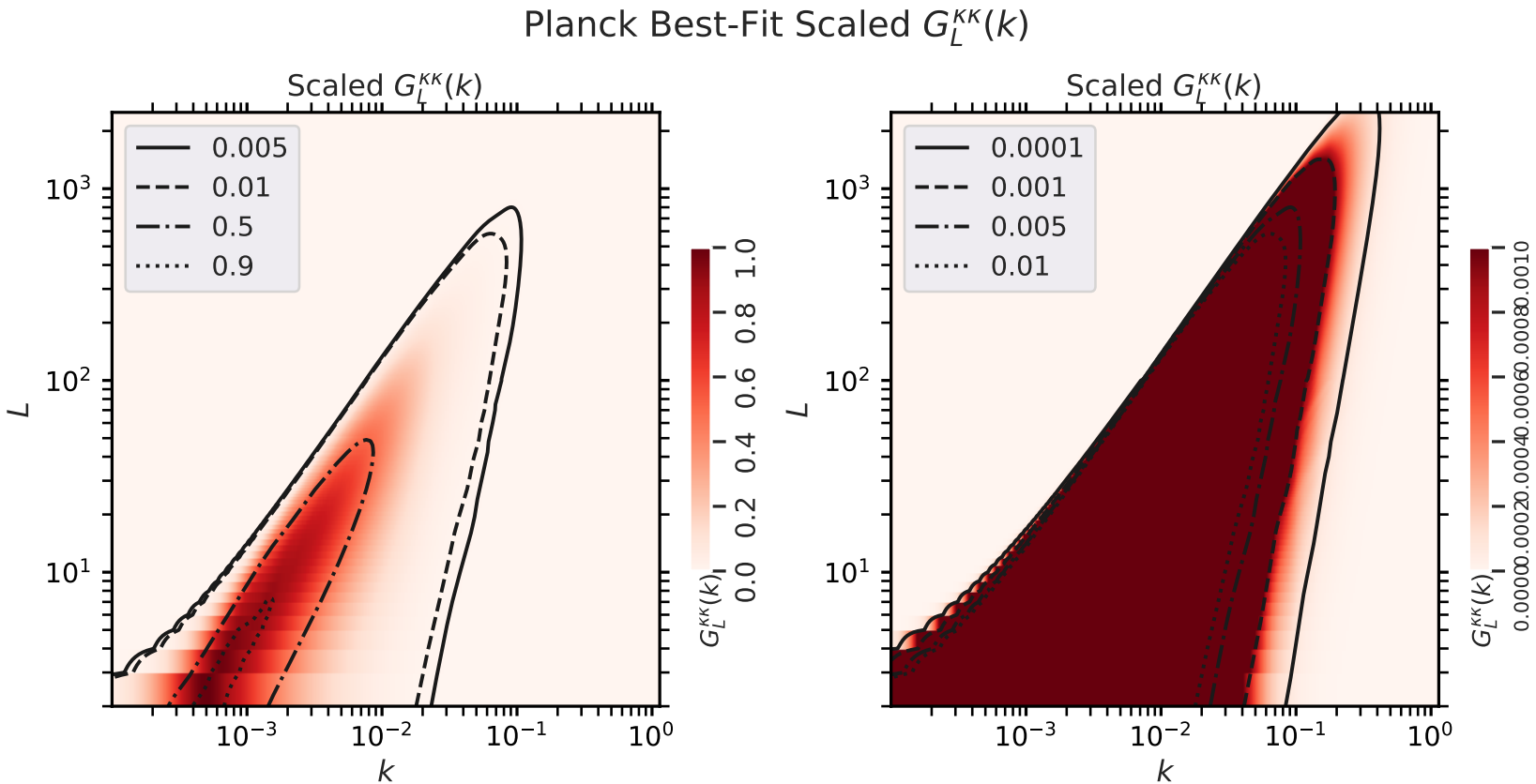

Figure 54: This plot shows a topdown view of the scaled transfer function given by $G_L^{\kappa\kappa}(k)/G_L^{\kappa\kappa}(k)_{max}$. The first plot shows the function with the complete power range 0 to 1 on the colorbar and 4 power level contours. The second plot shows the function in a power range 0 upto 0.001 on the colorbar with 4 power level contours.

$P_R(k)$ and $C_L^{\kappa\kappa}$ Reconstruction Error

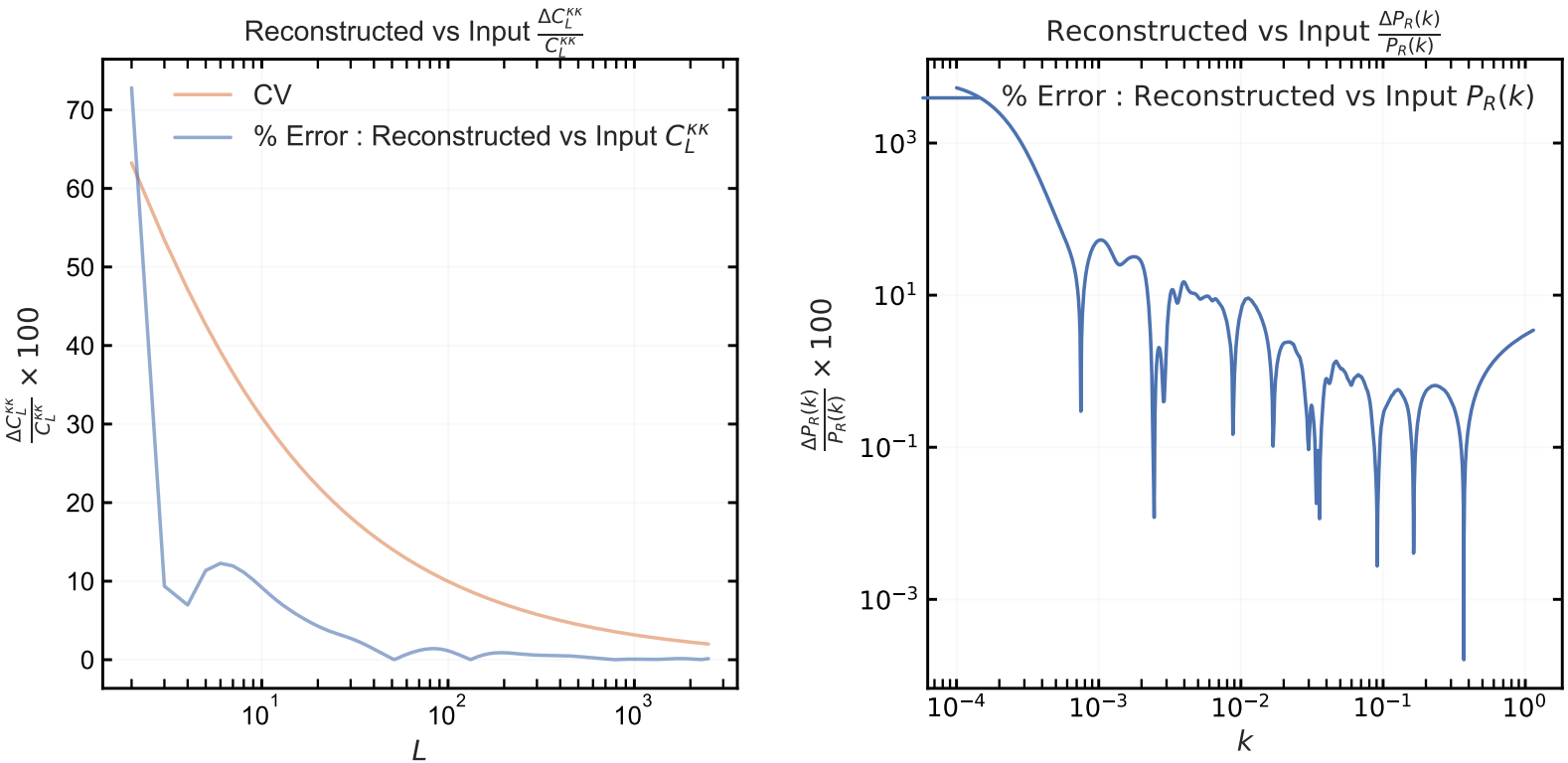

Figure 55: The two figures show the relative % error between the reconstructed $C_L^{\kappa\kappa}$ vs data realisation $C_L^{\kappa\kappa}$, and the reconstructed $P_R(k)$ vs input Power Law $P_R(k)$

Sparse $P_R(k)$ and $C_L^{\kappa\kappa}$ Reconstruction Error

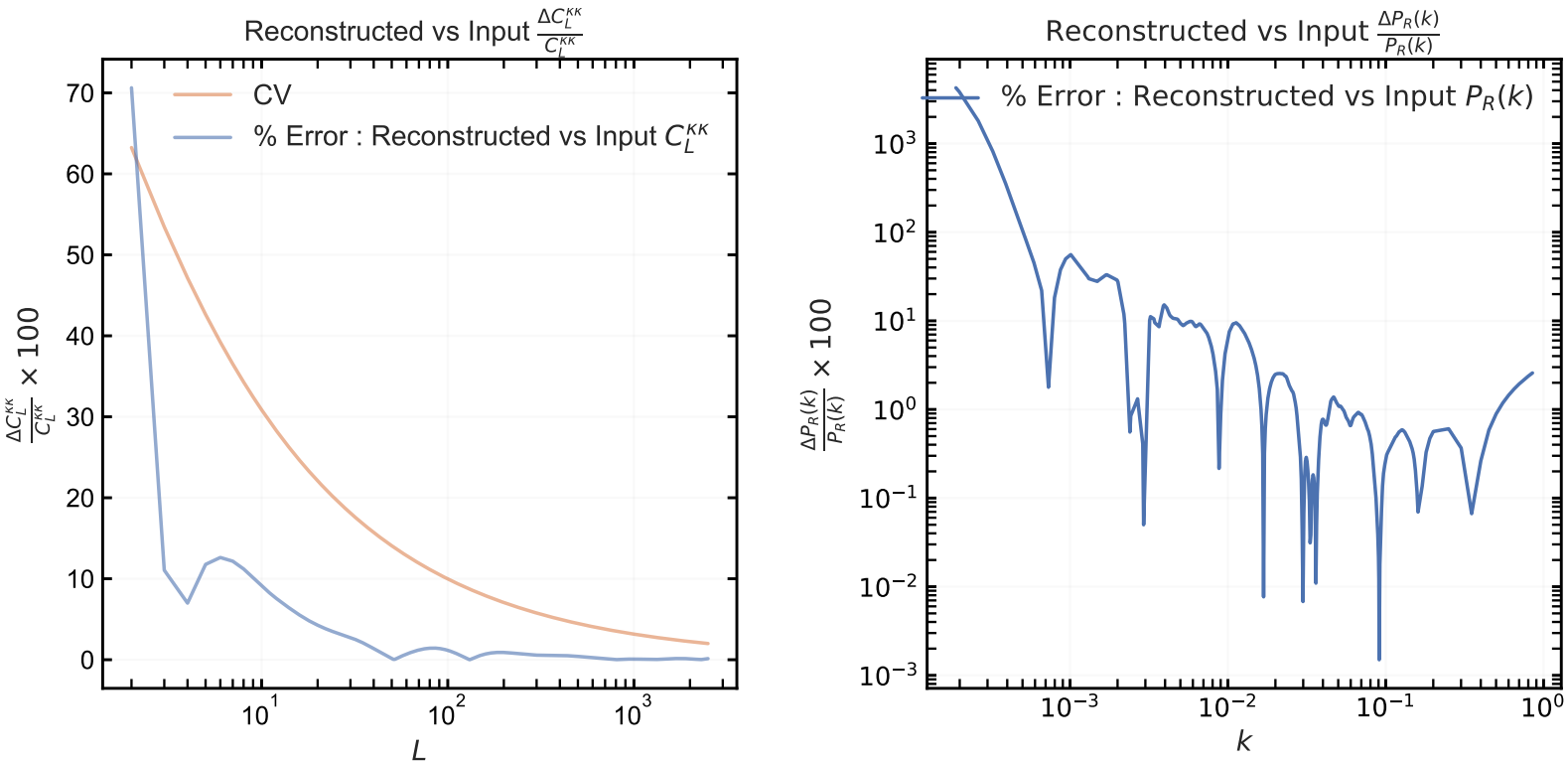

Figure 56: The two figures show the relative % error between the reconstructed $C_L^{\kappa\kappa}$ vs data realisation $C_L^{\kappa\kappa}$, and the reconstructed $P_R(k)$ vs input Power Law $P_R(k)$

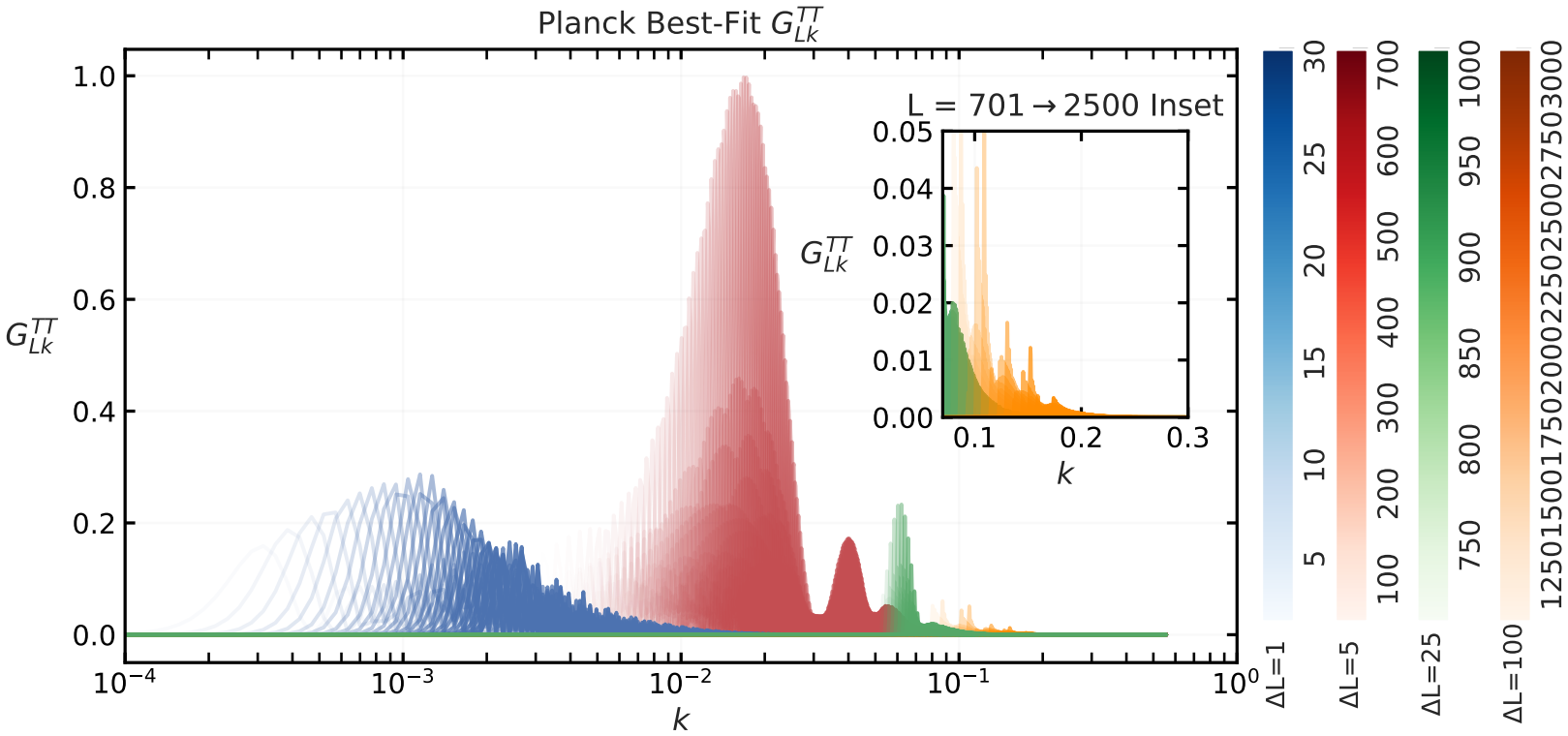

Figure 57: plot of the Unlensed temperature anisotropy power spectrum kernel $G_L^{TT}(k)$.

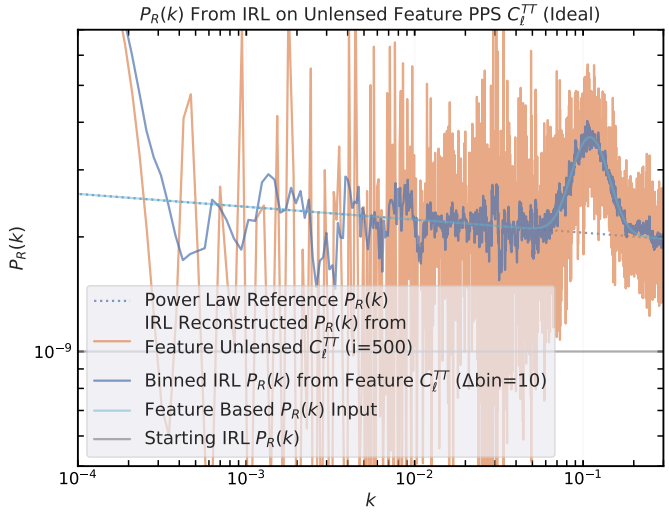
$P_R(k)$ From IRL on Unlensed Feature PPS C_ℓ^{TT} (Ideal)
$P_R(k)$
10^{-9}
10^{-4}
10^{-3}
10^{-2}
10^{-1}
k
Power Law Reference $P_R(k)$
IRL Reconstructed $P_R(k)$ from
Feature Unlensed C_ℓ^{TT} (i=500)
Binned IRL $P_R(k)$ from Feature C_ℓ^{TT} (Δbin=10)
Feature Based $P_R(k)$ Input
Starting IRL $P_R(k)$

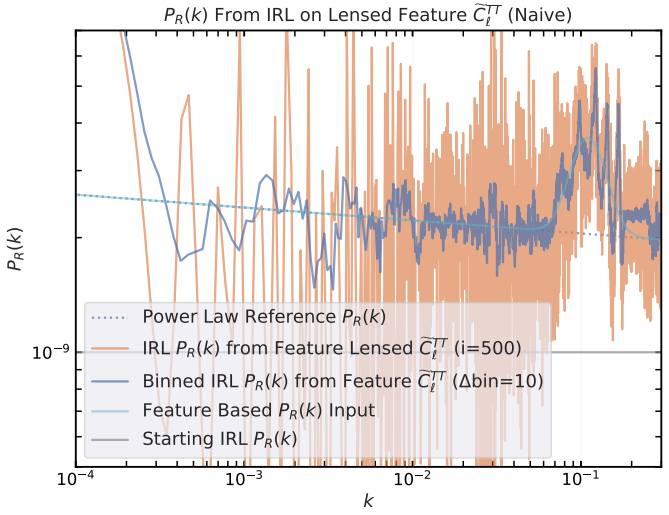
$P_R(k)$ From IRL on Lensed Feature $\widetilde{C}_\ell^{TT}$ (Naive)
$P_R(k)$
10^{-9}
10^{-4}
10^{-3}
10^{-2}
10^{-1}
k
Power Law Reference $P_R(k)$
IRL $P_R(k)$ from Feature Lensed $\widetilde{C}_\ell^{TT}$ (i=500)
Binned IRL $P_R(k)$ from Feature $\widetilde{C}_\ell^{TT}$ (Δbin=10)
Feature Based $P_R(k)$ Input
Starting IRL $P_R(k)$

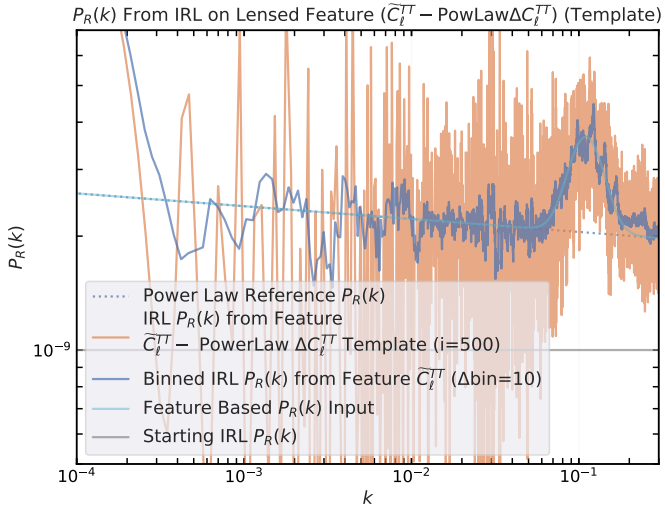
$P_R(k)$ From IRL on Lensed Feature ($\widetilde{C}_\ell^{TT}$ − PowLawΔC_ℓ^{TT}) (Template)
$P_R(k)$
10^{-9}
10^{-4}
10^{-3}
10^{-2}
10^{-1}
k
Power Law Reference $P_R(k)$
IRL $P_R(k)$ from Feature
$\widetilde{C}_\ell^{TT}$ − PowerLaw ΔC_ℓ^{TT} Template (i=500)
Binned IRL $P_R(k)$ from Feature $\widetilde{C}_\ell^{TT}$ (Δbin=10)
Feature Based $P_R(k)$ Input
Starting IRL $P_R(k)$

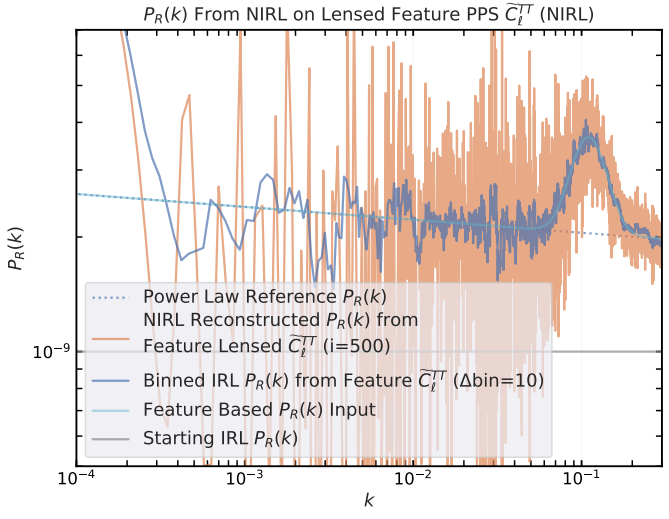
$P_R(k)$ From NIRL on Lensed Feature PPS $\widetilde{C}_\ell^{TT}$ (NIRL)
$P_R(k)$
10^{-9}
10^{-4}
10^{-3}
10^{-2}
10^{-1}
k
Power Law Reference $P_R(k)$
NIRL Reconstructed $P_R(k)$ from
Feature Lensed $\widetilde{C}_\ell^{TT}$ (i=500)
Binned IRL $P_R(k)$ from Feature $\widetilde{C}_\ell^{TT}$ (Δbin=10)
Feature Based $P_R(k)$ Input
Starting IRL $P_R(k)$

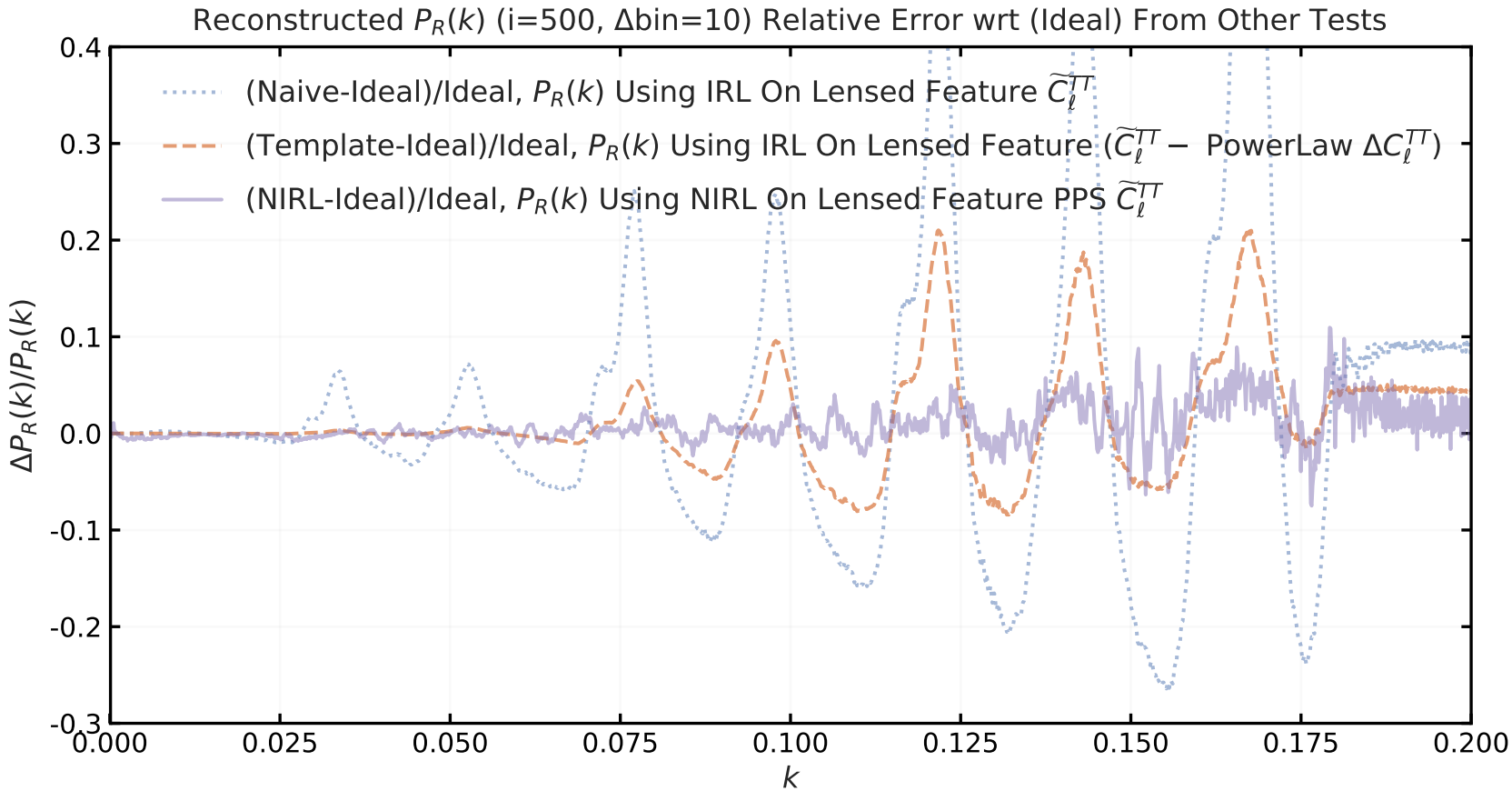

Figure 59: The figure displays the relative error of the 4 $P_R(k)$ reconstructions from the previous figures, with respect to first reconstruction, over 500 RL iterations.

Lensing Simulation

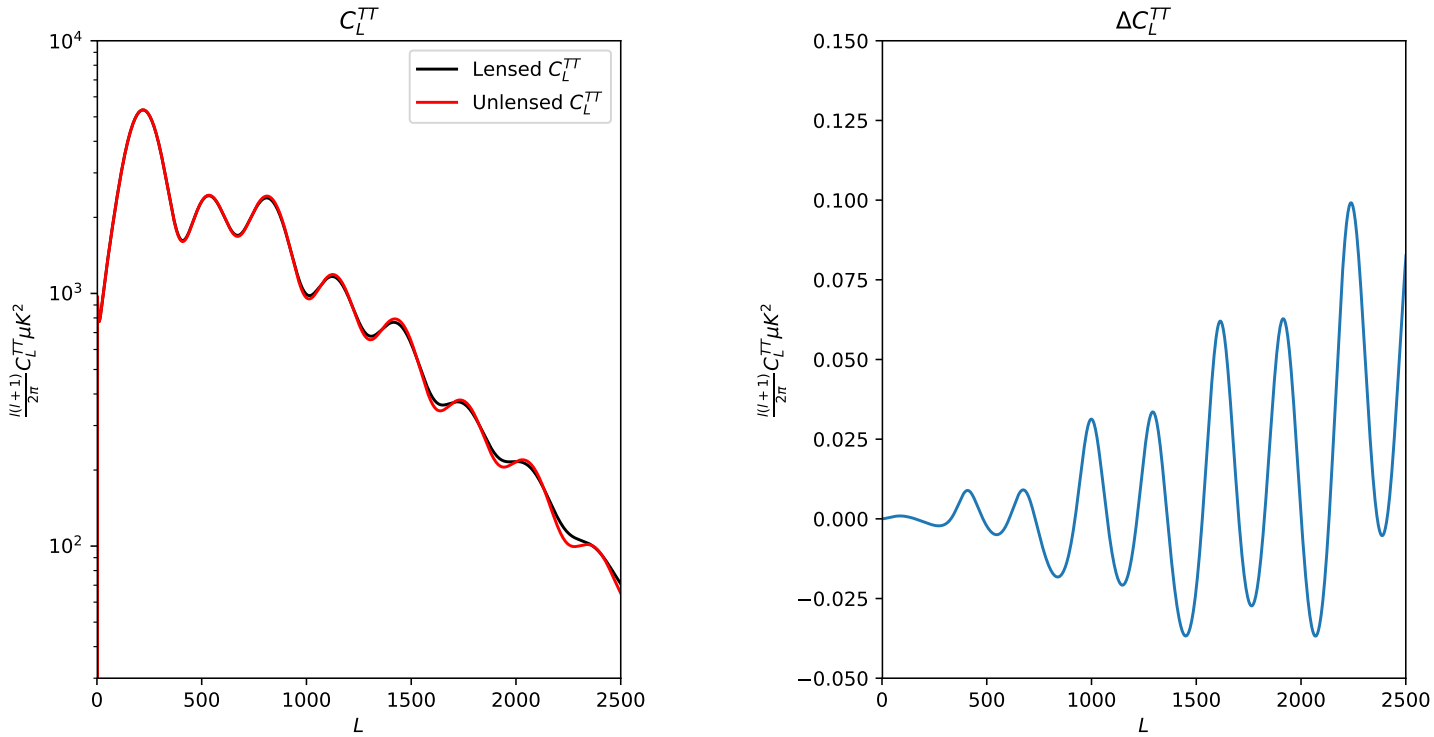

Figure 60: Lensed and unlensed power spectrum and the fractional change in power due to lensing at different scales. CAMB

Lensing Potential Power Spectrum

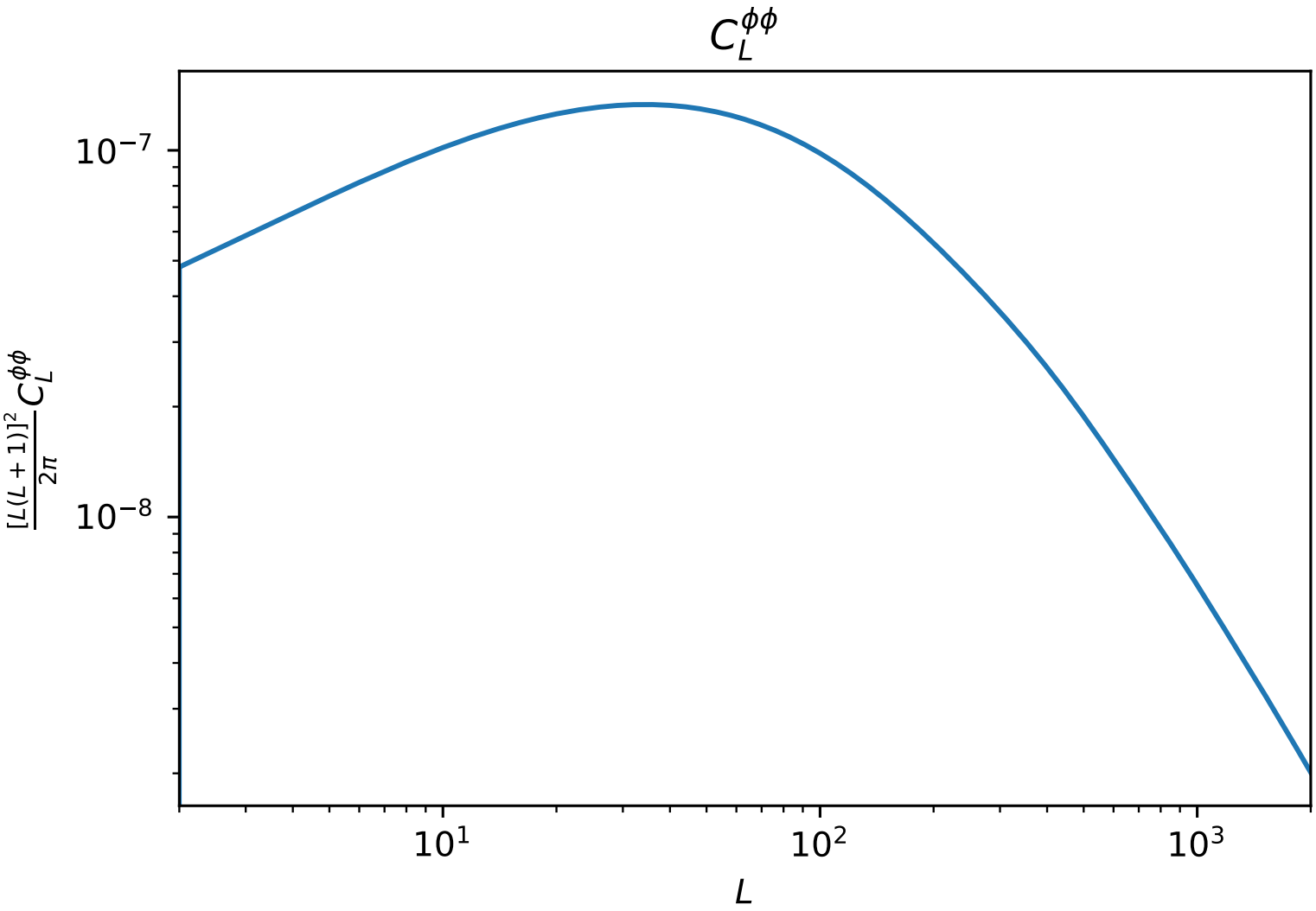

Figure 61: Plot of $C_l^{\phi\phi}$. Power dominates at low l. This means that large scale structures exist at large temperature-space angular scales, which cause the lensing effect to smoothen the peaks and valleys of the unlensed CMB anisotropy power spectrum at smaller temperature-space angular scales.

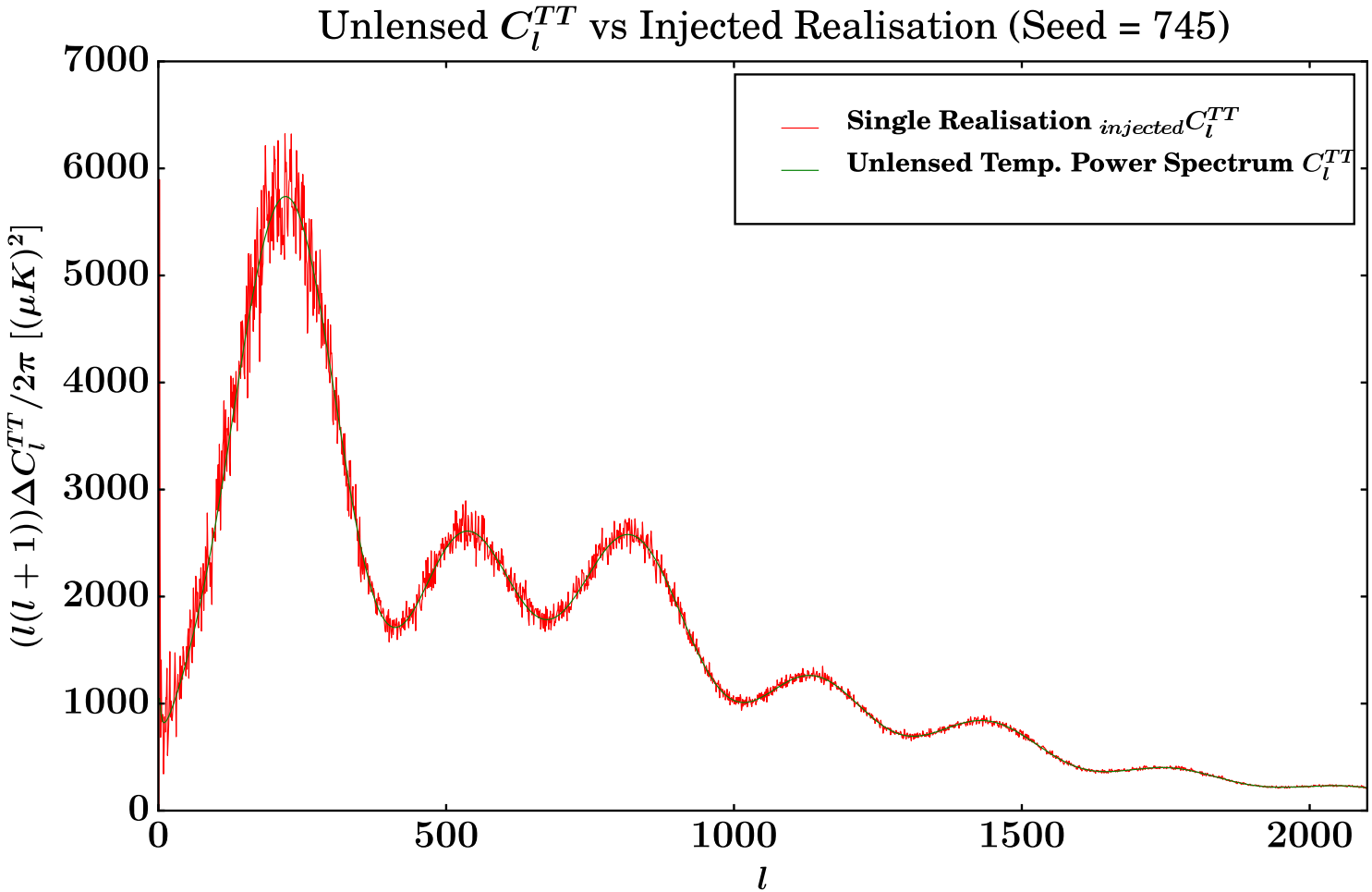

Figure 62: Comparison of the unlensed temperature map power spectrum for a generated realisation $\widehat{C}_L^{TT}$ with Healpix RNG seed 745 (red) vs input theoretical C_L^{TT} (green)

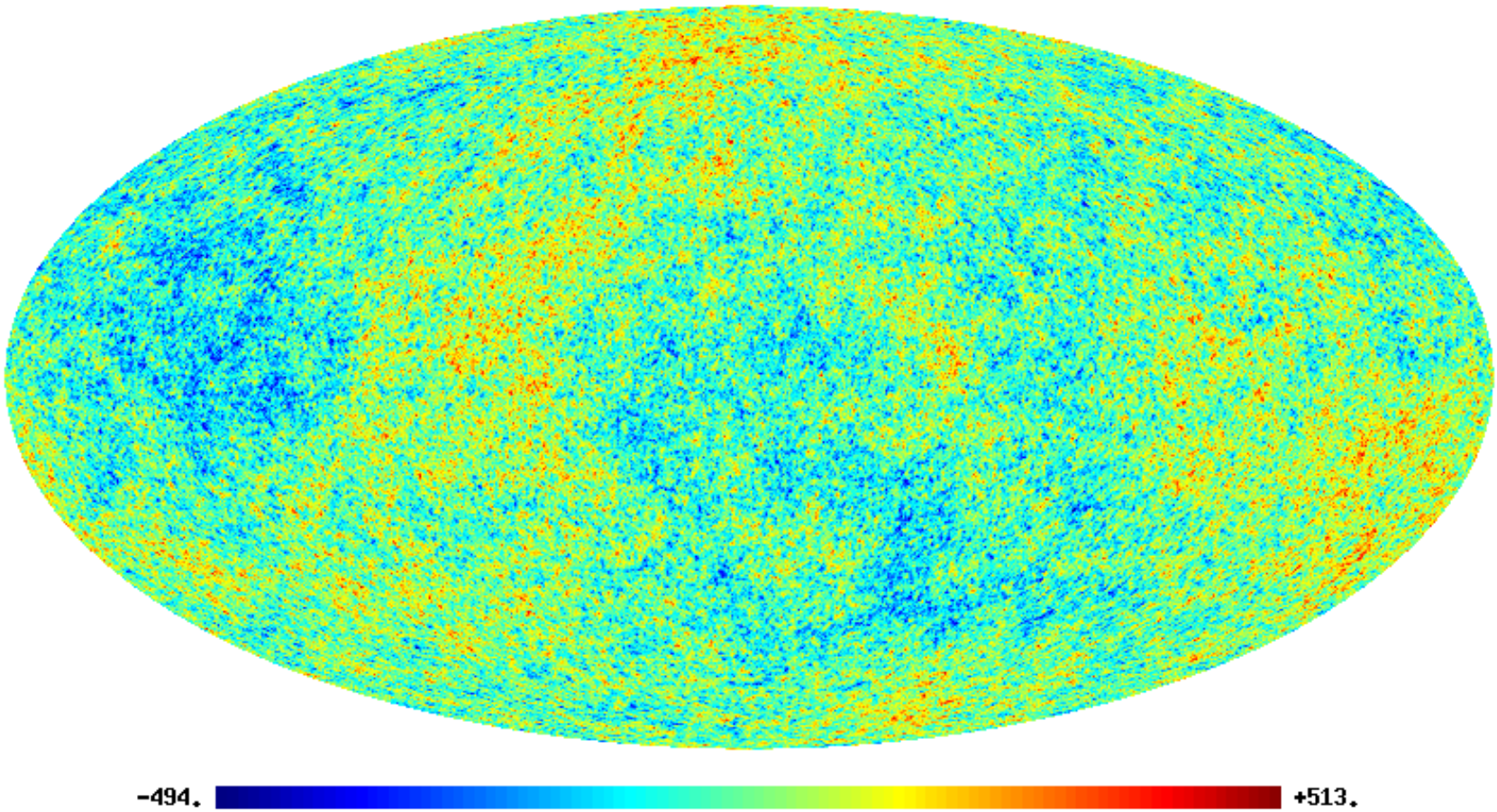

Figure 63: The unlensed and statistically isotropic CMB temperature map is shown corresponding to the realisation Healpix seed = 745 for which we have seen the two point angular power spectrum realisation in the previous image.

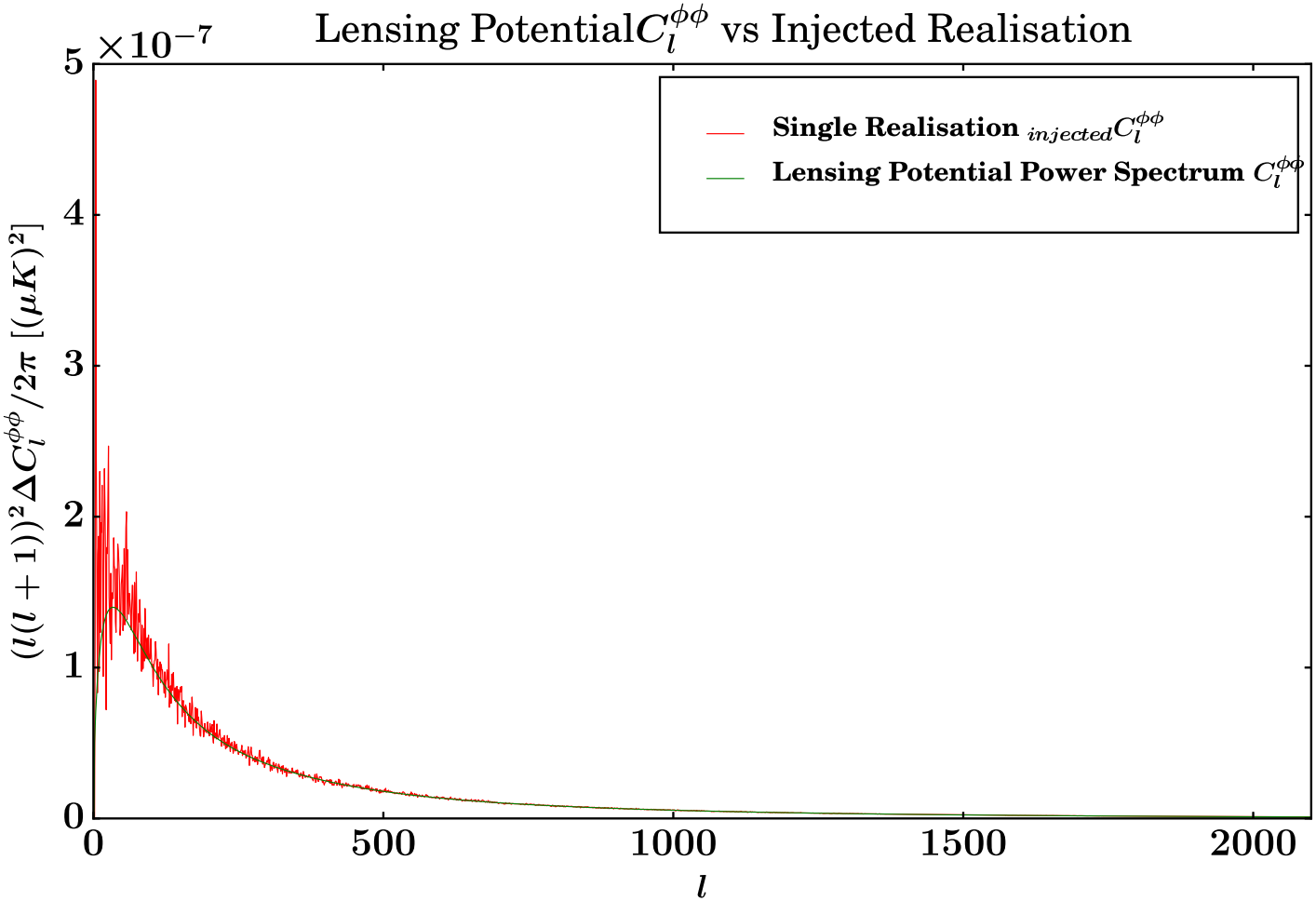

Figure 64: Plot showing comparison between theoretical $C_l^{\phi\phi}$ (green) and the reconstructed $\widehat{C}_l^{\phi\phi}$ (red) overlaid

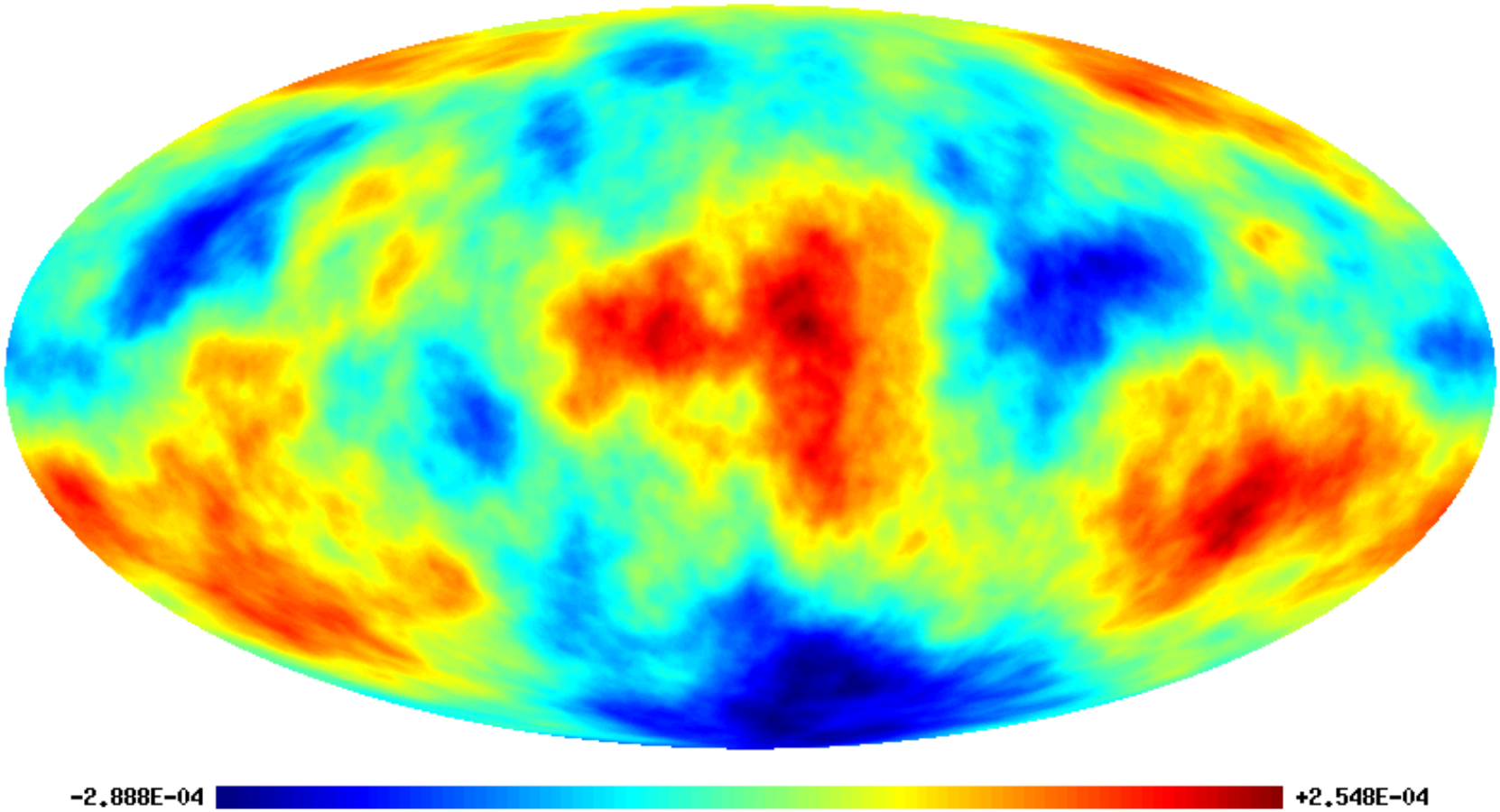

Figure 65: The realspace projected 2D weak lensing potential map is shown corresponding to the realisation Healpix seed = 745 for which we have seen the two point angular power spectrum realisation in the earlier image.

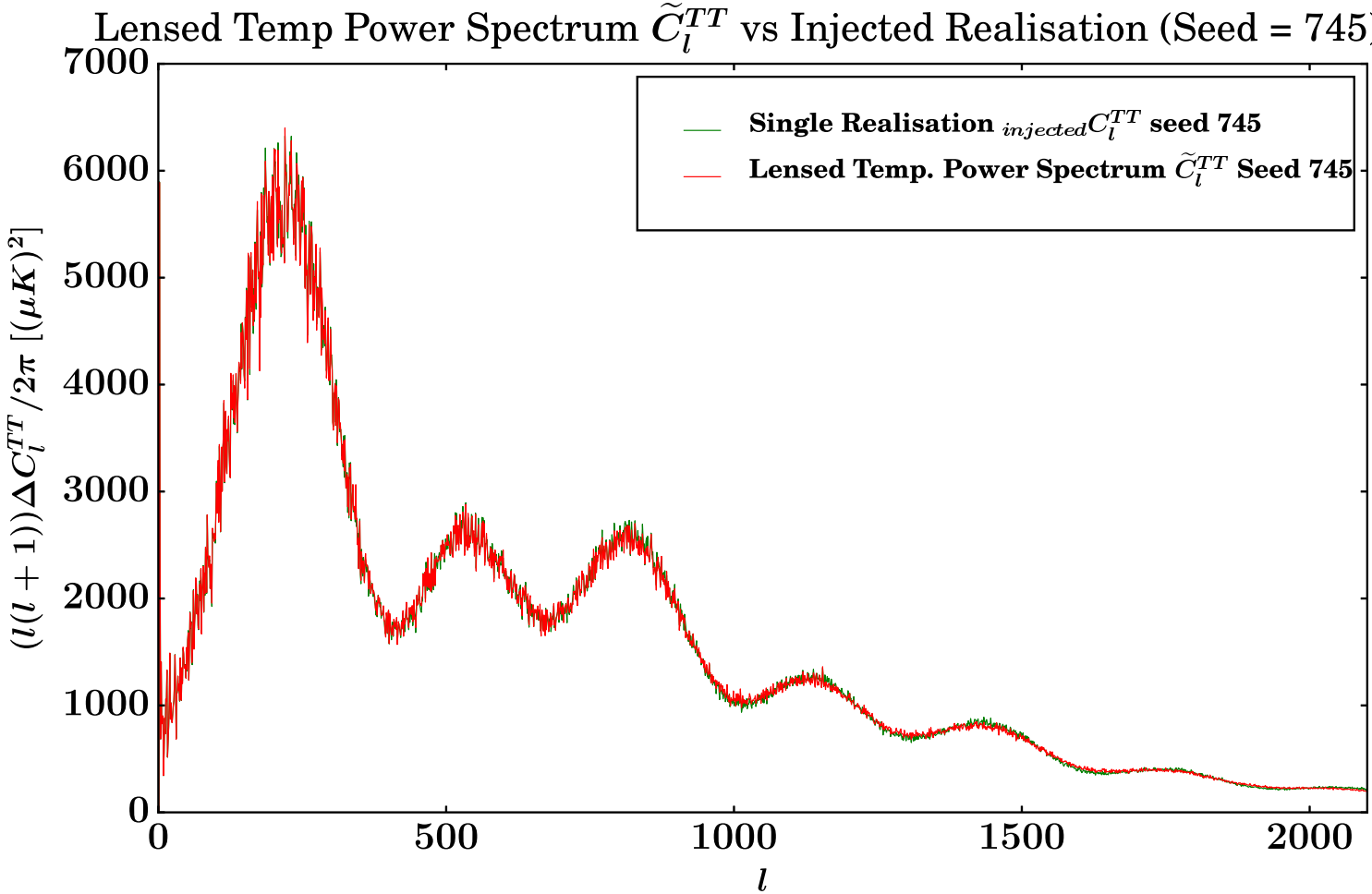

Figure 66: A comparison between the reconstructed angular power spectrum $\widehat{C}_L^{TT}$ (green) of the input unlensed CMB vs the reconstructed power spectrum $\widehat{\widetilde{C}}_L^{TT}$ (red) of output lensed CMB generated using Lenspix.

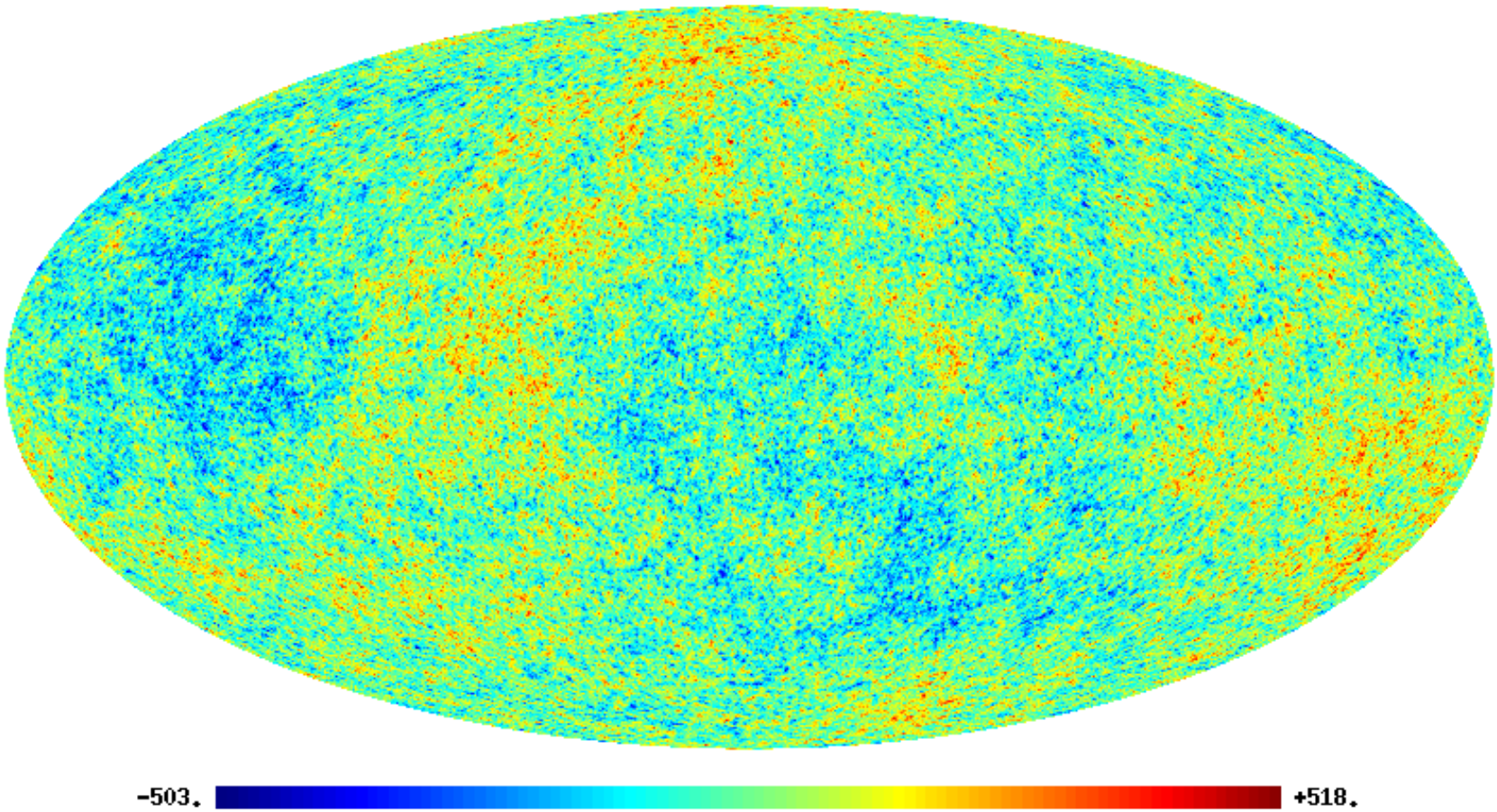

Figure 67: The lensed output map for the sample that we have been studying with unlensed CMB realisation seed = 745.

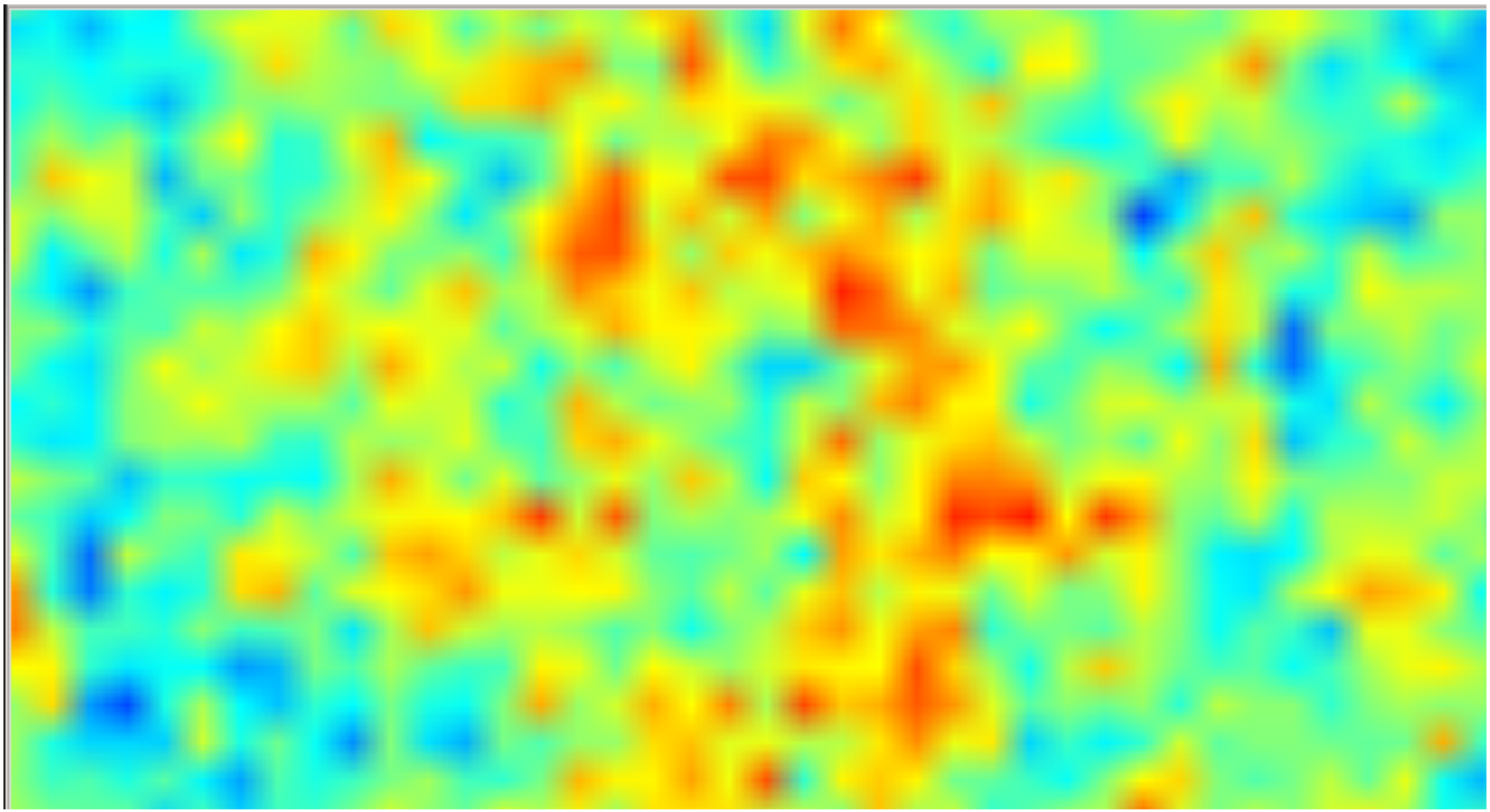

Figure 68: A zoomed section of the unlensed CMB temperature map from figure 63.

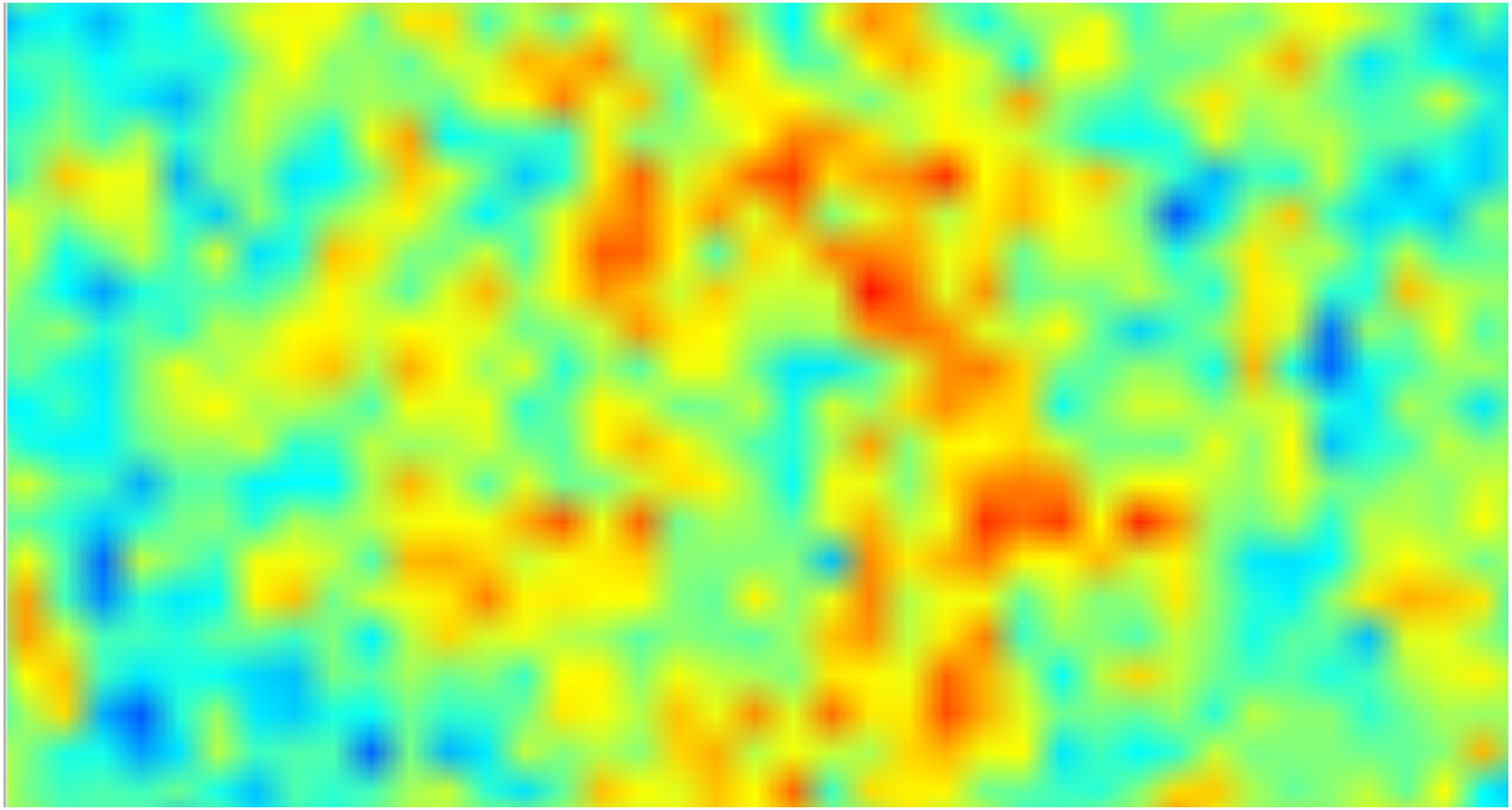

Figure 69: Zoomed section of the lensed CMB temperature map from figure 67. Refer to previous image for comparison.

Biposh First Order Lensing

We use the harmonic basis Taylor expansion

$$\widetilde{\Theta}_{lm} = \Theta_{lm} + \sum_{\substack{l_1 m_1 \\ l_2 m_2}} \Theta_{l_2 m_2} \phi_{l_1 m_1} I^{m m_1 m_2}_{l l_2 l_2} + \frac{1}{2} \sum_{\substack{l_1 m_1 \\ l_2 m_2}} \sum_{l_3 m_3} \phi_{l_1 m_1} \phi_{l_2 m_2} \Theta_{l_3 m_3} J^{m m_1 m_2 m_3}_{l l_1 l_2 l_3}$$
$$+ \frac{1}{6} \sum_{\substack{l_1 m_1 \\ l_2 m_2 \\ l_3 m_3}} \sum_{l_4 m_4} \phi_{l_1 m_1} \phi_{l_2 m_2} \phi_{l_3 m_3} \Theta_{l_4 m_4} K^{m m_1 m_2 m_3 m_4}_{l l_1 l_2 l_3 l_4}$$

To get the lensed Biposhes

$$\begin{aligned}
\mathcal{A}^{LM}_{ll'}|_{obs} &= \sum_{mm'} \langle \widetilde{\Theta}_{lm} \widetilde{\Theta}_{l'm'} \rangle (-1)^{m'} \mathcal{C}^{LM}_{lml'-m'} \\
&= \mathcal{A}^{LM}_{ll'}|_{S.I.} + \mathcal{A}^{LM}_{ll'}|_{\phi} + \mathcal{A}^{LM}_{ll'}|_{\phi\phi} + \mathcal{A}^{LM}_{ll'}|^{(a)}_{\phi^2} + \mathcal{A}^{LM}_{ll'}|^{(b)}_{\phi^2} \\
&+ \mathcal{A}^{LM}_{ll'}|^{(a)}_{\phi\phi^2} + \mathcal{A}^{LM}_{ll'}|^{(b)}_{\phi^2\phi} + \mathcal{A}^{LM}_{ll'}|^{(a)}_{\phi^3} + \mathcal{A}^{LM}_{ll'}|^{(b)}_{\phi^3}
\end{aligned} \tag{69}$$

Minimum Variance Estimator in Biposh

$$\lambda \;=\; 4 w^{L}_{ll'} \frac{C_l^{TT} C_{l'}^{TT}}{(\mathcal{K}^{L}_{ll'}|_{\phi})^2} \tag{70}$$

$$w^{L}_{ll'} \;=\; \frac{(\mathcal{K}^{L}_{ll'}|_{\phi})^2}{C_l^{TT} C_{l'}^{TT}} \Bigg/ \left[\sum_{ll'} \frac{(\mathcal{K}^{L}_{ll'}|_{\phi})^2}{C_l^{TT} C_{l'}^{TT}} \right] \tag{71}$$

$$N^{(0)}_{L} \;=\; 2 \Bigg/ \left[\sum_{ll'} \frac{(\mathcal{K}^{L}_{ll'}|_{\phi})^2}{C_l^{TT} C_{l'}^{TT}} \right] \tag{72}$$